Estimating the lateral transfer of organic carbon through the European river network using a land surface model

Haicheng Zhang, Ronny Lauerwald, Pierre Regnier, Philippe Ciais, Kristof van Oost, Victoria Naipal, Bertrand Guenet, Wenping Yuan

https://doi.org/10.5194/esd-2022-4
Preprint. Discussion started: 1 February 2022

Earth System Dynamics
Discussions
Open Access
EGU

Estimating the lateral transfer of organic carbon through the European river network using a land surface model

Haicheng Zhang[1*], Ronny Lauerwald[2], Pierre Regnier[1], Philippe Ciais[3], Kristof Van Oost[4], Victoria Naipal[5], Bertrand Guenet[3], Wenping Yuan[6]

[1]Department Geoscience, Environment & Society-BGEOSYS, Université libre de Bruxelles, 1050 Bruxelles, Belgium

[2] Université Paris-Saclay, INRAE, AgroParisTech, UMR ECOSYS, 78850, Thiverval-Grignon, France

[3]Laboratoire des Sciences du Climat et de l'Environnement, IPSL-LSCE CEA/CNRS/UVSQ, Orme des Merisiers, 91191, Gif sur Yvette, France

[4]UCLouvain, TECLIM - Georges Lemaître Centre for Earth and Climate Research, Louvain-la-Neuve, Belgium

[5]EcoAct/ ATOS, 35 rue de miromesnil, 75008, Paris, France

[6]School of Atmospheric Science, Sun Yat-sen University, Guangzhou, Guangdong, 510275, China

Correspondence to: Haicheng Zhang (*haicheng.zhang@ulb.be*)

https://doi.org/10.5194/esd-2022-4
Preprint. Discussion started: 1 February 2022

Earth System Dynamics
Discussions
Open Access
EGU

Abstract. Lateral carbon transport from soils to the ocean through rivers has been acknowledged as a key component of global carbon cycle, but is still neglected in most global land surface models (LSMs). Fluvial transport of dissolved organic carbon (DOC) and CO_2 has been implemented in the ORCHIDEE LSM, while erosion-induced delivery of sediment and particulate organic carbon (POC) from land to river was implemented in another version of the model. Based on these two developments, we take the final step towards the full representation of biospheric carbon transport through the land-river continuum. The newly developed model, called ORCHIDEE-$C_{lateral}$, simulates the complete lateral transport of water, sediment, POC, DOC and CO_2 from land to sea through the river network, the deposition of sediment and POC in the river channel and floodplains, and the decomposition of POC and DOC in transit. We parameterized and evaluated ORCHIDEE-$C_{lateral}$ using observation data in Europe. The model satisfactorily reproduces the observed riverine discharges of water and sediment, bankfull flows and sediment delivery rate from land to river, as well as the observed concentrations of organic carbon in rivers. Application of ORCHIDEE-$C_{lateral}$ for Europe reveals that the lateral carbon transfer affects land carbon dynamics in multiple ways and omission of this process in LSMs may result in significant biases in the simulated regional land carbon budgets. Overall, this study presents a useful tool for simulating large scale lateral carbon transfer and for predicting the feedbacks between lateral carbon transfer and future climate and land use changes.

https://doi.org/10.5194/esd-2022-4
Preprint. Discussion started: 1 February 2022


Earth System Dynamics Discussions

1 Introduction

Lateral transfer of organic carbon along the land-river-ocean continuums, involving both spatial redistribution of terrestrial organic carbon and the vertical land-atmosphere carbon exchange, has been acknowledged as a key component of the global carbon cycle (Ciais et al., 2013; Ciais et al., 2021; Drake et al., 2018; Regnier et al., 2013). Erosion of soils and the associated organic carbon, but also leaching of dissolved organic carbon (DOC), represent a non-negligible leak in the terrestrial carbon budget and a substantial source of allochthonous organic carbon to inland waters and oceans (Battin et al., 2009; Cole et al., 2007; Raymond et al., 2013; Regnier et al., 2013). As a result of soil aggregate breakdown and desorption, the accelerated mineralization of these eroded and leached soil carbon loads leads to considerable CO_2 emission to the atmosphere (Chappell et al., 2016; Lal, 2003; Van Hemelryck et al., 2011). Meanwhile, the organic carbon that is redeposited and buried in floodplains and lakes might be preserved for a long time, thus creating a CO_2 sink (Stallard, 1998; Van Oost et al., 2007; Wang et al., 2010). In addition, lateral redistribution of soil material can alter land-atmosphere CO_2 fluxes indirectly by affecting soil nutrient availability, terrestrial vegetation productivity and physiochemical properties of inland and coastal waters (Beusen et al., 2005; Vigiak et al., 2017).

Although the important role of lateral carbon transfer in the global carbon cycle has been widely recognized, to date, the estimates of land carbon loss to inland waters, the fate of the terrestrial organic carbon within inland waters, as well as the net effect of lateral carbon transfer on land-atmosphere CO_2 fluxes remain largely uncertain (Berhe et al., 2007; Doetterl et al., 2016; Lal, 2003; Stallard, 1998; Wang et al., 2014b; Zhang et al., 2014). Existing estimates of global carbon loss from soils to inland waters vary from 1.1 to 5.1 Pg ($=10^{15}$ g) C per year (yr^{-1}) (Cole et al., 2007; Drake et al., 2018), and the estimated net impact of global lateral carbon redistribution on land-atmosphere carbon budget ranges from an uptake of atmospheric CO_2 by 1 Pg C yr^{-1} to a land CO_2 emission of 1 Pg C yr^{-1} (Lal, 2003; Stallard, 1998; Van Oost et al., 2007; Wang et al., 2017). A reliable model which is able to explicitly simulate the lateral carbon along the land-river continuum and also the interactions between these lateral processes and the comprehensive terrestrial carbon cycle, would thus be necessary for predicting changes in the global carbon cycle more accurately.

https://doi.org/10.5194/esd-2022-4
Preprint. Discussion started: 1 February 2022


Earth System Dynamics Discussions

Global land surface models (LSMs) are important tools to simulate the feedbacks between terrestrial carbon cycle, increasing atmospheric CO_2, and climate and land use change. However, the lateral carbon transfer, especially for the particulate organic carbon (POC), is still missing or incompletely represented in existing LSMs (Lauerwald et al., 2017; Lauerwald et al., 2020; Lugato et al., 2016; Naipal et al., 2020; Nakhavali et al., 2021; Tian et al., 2015). It has been hypothesized that the exclusion of lateral carbon transfer in LSMs implies a significant bias in the simulated global land carbon budget (Ciais et al., 2013; Ciais et al., 2021; Janssens et al., 2003). For instance, the study of Nakhavali et al. (2021) suggested that about 15% of the global terrestrial net ecosystem production is exported to inland waters as leached DOC. Lauerwald et al. (2020) showed that the omission of lateral DOC transfer in LSM might lead to significant underestimation (8.6%) of the net uptake of atmospheric carbon in the Amazon basin while terrestrial carbon storage changes in response to the increasing atmospheric CO_2 concentrations were overestimated.

Over the past decade, a number of LSMs has been developed which represent leaching of DOC from soils (Nakhavali et al. 2018, Kicklighter et al. 2013) or the full transport of DOC through the land-river continuum (Lauerwald et al., 2017; Tian et al., 2015). However, the erosion-induced transport of POC, which is maybe even more important than the DOC transport in terms of lateral carbon flux (Lal., 2003; Tian et al., 2015; Tan et al., 2017), is still not or poorly represented in LSMs. The explicit simulation of the complete transport process of POC at large spatial scales is still a major challenge, due to the complexity of the processes involved, including erosion-induced sediment and POC delivery to rivers, deposition of sediment and POC in river channels and floodplains, re-detachment of the previously deposited sediments and POC, decomposition and transformation of POC in riverine and flooding waters, as well as the changes of soil profile caused by erosion and deposition (Doetterl et al., 2016; Naipal et al., 2020; Zhang et al., 2020).

Several recent model developments have led to the implementation of the lateral transfer of POC in large-scale LSMs. Despite this, there are still some inevitable limitations in these implementations. The Dynamic Land Ecosystem Model (DLEM v2.0, Tian et al., 2015) is able to simulate the erosion-induced POC loss from soil to river and the transport and decomposition of POC in river networks. However, it does not represent the POC deposition in floodplains, nor

https://doi.org/10.5194/esd-2022-4
Preprint. Discussion started: 1 February 2022

the impacts of soil erosion and floodplain deposition on the vertical profiles of soil organic carbon (SOC). The Carbon Erosion DYNAMics model (CE-DYNAM, Naipal et al., 2020) simulates erosion of SOC and its re-deposition on the toe-slope or floodplains, transport of POC along river channels, as well as the impact on SOC dynamics at the eroding and deposition sites. However, running at annual time scale, it mostly addresses the centennial timescale and does not represent deposition and decomposition of POC in river channels. Moreover, CE-DYNAM was only applied over the Rhine catchment and has not been fully coupled into a land surface model, therefore excluding the feedbacks of soil erosion on the fully coupled land and aquatic carbon cycles. There are of course more dedicated hydrology and soil erosion models that explicitly simulate the complete transport, deposition and decomposition processes of POC in small river basins (e.g. Jetten et al., 2003; Nearing et al., 1989; Neitsch et al., 2011). However, it is difficult to apply these models at large spatial scales (e.g. continental or global scale) due to the limited availability of forcing data (e.g. geometric attributes of river channel), suitable model parameterization and computational capacity. Moreover, these models have limited capability of representing the full terrestrial C cycle in response to climate change, increasing atmospheric CO_2 and land use change. Therefore, basin-scale models are not an option to assess the impact of soil erosion on the large-scale terrestrial C budget in response to global changes.

Here we describe the development, application and evaluation of a new branch of the ORCHIDEE LSM (Krinner et al., 2005), hereafter ORCHIDEE-$C_{lateral}$, that can be used to simulate the complete lateral transfer processes of water, sediment, POC and DOC along the land-river-ocean continuum at large spatial scale (e.g. continental and global scale). In previous studies, the leaching and fluvial transfer of DOC and the erosion-induced delivery of sediment and POC from upland soil to river network have been implemented in two different branches of the ORCHIDEE LSM (Lauerwald et al., 2017; Zhang et al., 2020). For this new branch, we first merged these two branches, and subsequently implemented the fluvial transfer of sediment and POC in the coupled model. ORCHIDEE-$C_{lateral}$ is calibrated and evaluated using observation data of runoff, bankfull flow, and riverine loads and concentrations of sediment, POC and DOC across Europe. By applying the calibrated model at European scale, we estimate the magnitude and spatial distribution of the lateral carbon transfer in European catchments during the period 1901-2014, as well as the potential impacts of lateral carbon transfer on the land carbon balance. Comparing simulations results to those of an alternative simulation run with lateral displacement

https://doi.org/10.5194/esd-2022-4
Preprint. Discussion started: 1 February 2022


Earth System Dynamics Discussions

of C deactivated, we finally quantify the biases in simulated land C budgets that arise ignoring the lateral transfers of C along the land-river continuum.

2 Model development and evaluation

2.1 ORCHIDEE land surface model

The ORCHIDEE LSM comprehensively simulates the cycling of energy, water and carbon in terrestrial ecosystems (Krinner et al., 2005). The hydrological processes (e.g. rainfall interception, evapotranspiration and soil water dynamics) and plant photosynthesis in ORCHIDEE are simulated at a time step of 30 minutes. The carbon cycle processes (e.g. maintenance and growth respiration, carbon allocation, litter decomposition, SOC dynamics, plant phenology and mortality) are simulated at daily time step. In its default configuration, ORCHIDEE represents vegetation by 13 plant functional types (PFTs), with eight PFT for forests, two for grasslands, two for croplands, and one for bare soil. Given appropriate land cover maps and parametrization, the number of PFTs to be represented can however be adapted (Zhang et al., 2020).

Our previous implementations of lateral DOC transfer (Lauerwald et al., 2017) and of POC delivery from upland to river network (Zhang et al., 2020) were both based on the ORCHIDEE branch ORCHIDEE-SOM (Camino-Serrano et al., 2018), which provides a depth-dependent description of the water and carbon dynamics in soil column. In specific, the vertical soil profile in ORCHIDEE-SOM is described by an 11-layer discretization of a 2 m soil column (Camino-Serrano et al., 2018). Water flows between adjacent soil layers are simulated using the Fokker–Planck equation that resolves water diffusion in non-saturated conditions (Campoy et al., 2013; Guimberteau et al., 2018). Free gravitational drainage occurs in the lowest soil layer when actual soil water content is higher than the residual water content (Campoy et al., 2013). Following the CENTURY model (Parton et al., 1988), ORCHIDEE-SOM subdivides the particulate organic carbon stored in soil into two litter pools (metabolic and structural) and three SOC pools (active, slow and passive) that differ in their respective turnover times. The decomposition of each carbon pool is calculated by first order kinetics based on the corresponding turnover time, soil moisture and temperature as controlling factors, as well as the priming effects of fresh organic matter (Guenet et al., 2018; Guenet et al., 2016). Soil DOC is represented by a labile and a stable

https://doi.org/10.5194/esd-2022-4
Preprint. Discussion started: 1 February 2022

153 DOC pools, with a high and low turnover rate, respectively. Each DOC pool may be in the soil
154 solution or adsorbed on the mineral matrix. The products of litter and SOC decomposition go to
155 free DOC, which in turn is decomposed following first order kinetics (Kalbitz et al., 2003) and
156 returns back to SOC. "The free DOC can then be adsorbed to soil minerals or remain in solution
157 following an equilibrium distribution coefficient (Nodvin et al., 1986), which depends on soil
158 properties (clay and pH). Adsorbed DOC is assumed to be protected and thus is neither
159 decomposed nor transported within the soil column. Free DOC is subject to transport with the
160 water flux between layers calculated by the soil hydrological module of ORCHIDEE, i.e., by
161 advection. Also, SOC and DOC are subject to diffusion that is represented using the second
162 Fick's law of diffusion" (Camino-Serrano et al., 2018, p. 939). All the described processes occur
163 within each soil layer. At each time step, "the flux of DOC leaving the soil is calculated by
164 multiplying DOC concentrations in soil solution with the runoff (surface layer) and drainage
165 (bottom layer) flux simulated by the hydrological module" (Camino-Serrano et al., 2018, p. 939).
166 More detailed information about the simulation of soil hydrological and biogeochemical
167 processes in ORCHIDEE-SOM can be found in Guenet et al. (2016) and Camino-Serrano et al.
168 (2018).

169 **2.1.1 Lateral transfer of DOC and CO_2**

170 Lateral transfer of DOC and dissolved CO_2 from land to ocean through river network has been
171 implemented in the ORCHILEAK (Lauerwald et al., 2017), an ORCHIDEE branch developed
172 from ORCHIDEE-SOM. The adsorption, desorption, production, consumption and transport of
173 DOC within the soil column, as well as DOC export from soil along with surface runoff and
174 drainage in ORCHILEAK is simulated using the same method as ORCHIDEE-SOM. Besides the
175 decomposition of SOC and litter, ORCHILEAK also represents the contribution of wet and dry
176 deposition to soil DOC via throughfall. The direct DOC input from rainfall to aquatic DOC pools
177 is simulated based on the DOC concentration in rainfall and the area fraction of stream and
178 flooding waters in each basin. Simulation of the lateral transfer of DOC and CO_2 in river
179 networks, i.e. the transfer of DOC and CO_2 from one basin to another based on the stream flow
180 directions obtained from forcing file (0.5°, Table 1), follows the routing scheme of water
181 (Guimberteau et al., 2012). For each basin with floodplain (defined by forcing data), bankfull
182 flow occurs when stream volume in the river channel exceeds a threshold prescribed by the

https://doi.org/10.5194/esd-2022-4
Preprint. Discussion started: 1 February 2022

Earth System Dynamics Discussions

183 forcing file (Table 1). DOC and CO_2 in flooding waters can enter into soil DOC and CO_2 pools
184 along with the infiltrating water. On the contrary, DOC and CO_2 originated from the
185 decomposition of submerged litter and SOC in the floodplains are added to the overlying
186 flooding waters. Note that the turnover times of litter and SOC under flooding waters are
187 assumed to be three times of the litter and SOC turnover times in upland soil (Reddy & Patrick
188 Jr, 1975; Neckles & Neill, 1994; Lauerwald et al., 2017). After removing the infiltrated and
189 evaporated water, the amount of the remaining flooding water, as well as the DOC and dissolved
190 CO_2 returning to river channel at the end of each day is calculated based on a time constant of
191 flooding water (= 4.0 days, d'Orgeval et al., 2008) modified by basin-specific topographic index
192 (f_{topo}, unitless) (Lauerwald et al., 2017).
193
194 **Table 1.** List of forcing data needed to run ORCHIDEE-$C_{lateral}$ and the data used to evaluate the
195 simulation results. S_{res} and T_{res} are the spatial and temporal resolution of the forcing data,
196 respectively.

	Data	S_{res}	T_{res}	Data source
Forcing	Climatic forcing data (precipitation, temperature, incoming shortwave/longwave radiation, air pressure, wind speed, relative humidity)	0.5°	3 hour	GSWP3 database (Dirmeyerm et al., 2006)
	Land cover	0.5°	1 year	LUHa.rc2 database (Chini et al., 2014)
	Soil texture class	0.5°	–	Reynolds et al. (1999)
	Soil bulk density and pH	30″	–	HWSD v1.2 (FAO/IIASA/ISRIC/ISSCAS/JRC, 2012)
	Stream flow directions, topographic index (f_{topo})	0.5°	–	STN-30p (Vörösmarty et al., 2000)
	Area fraction of floodplains	250 m	–	GFPLAIN250m (Nardi et al., 2019)[a]
	Area fraction of river surface	0.5°	–	Lauerwald et al. (2015)
	Maximum water storage in river channel (S_{rivmax})	0.5°	–	Derived from pre-runs with ORCHIDEE-$C_{lateral}$ (see section 2.3)
	Reference sediment delivery rate (SED_{ref})	0.5°	–	Zhang et al. (2020)
	Digital Elevation Model (DEM)	3″	–	HydroSHEDS (Lehner et al., 2008) and GDEM v3 (Abrams et al., 2020)[b]
Validation	Riverine water discharge	–	1 day	GRDC[c]
	Bankfull flow	–	1 year	Schneider et al. (2011)
	Sediment delivery from upland to inland waters	100 m	1 year	Borrelli et al. (2018)
	Riverine sediment discharge	–	1 year	European Environment Agency[d] and publications[e]
	Riverine POC and DOC concentration	–	Instantaneous	GLORICH (Hartmann et al., 2019)
	SOC stock	30″	–	HWSD v1.2
		5′		GSDE (Shangguan et al., 2014)
		250 m		SoilGrids (Hengl et al., 2014)

https://doi.org/10.5194/esd-2022-4
Preprint. Discussion started: 1 February 2022

Earth System Dynamics Discussions

	10 km	S2017 (Sanderman et al., 2017)
	250 m	LandGIS[f]

[a] The GFPLAIN250m only covers the regions south of 60° N. We produced map of floodplain distribution in regions north of the 60° N using the same method for producing GFPLAIN250m (Nardi et al., 2019) based on the ASTER GDEM v3 database (Abrams et al., 2020). [b] The DEM data from HydroSHEDS and GDEM v3 are used to extract the topographic properties (e.g. location, area and average slope) of headwater basins in regions south and north of 60° N, respectively. [c] The Global Runoff Data Centre, 56068 Koblenz, Germany. [d] https://www.eea.europa.eu/data-and-maps/data/sediment-discharges. [e] Publications including Van Dijk & Kwaad, 1998; Vollmer & Goelz, (2006) and Reports of the DanubeSediment project (Sediment Management Measures for the Danube, http://www.interreg-danube.eu/approved-projects/danubesediment). [f] https://zenodo.org/record/2536040#.YC-QGo9KiUm.

DOC decomposition and CO_2 evasion in inland waters are simulated using a much fine integration time step of 6 minutes. The decomposition of DOC in stream and flooding waters is calculated based on the prescribed turnover times of labile (2 days) and refractory (80 days) DOC in waters (when temperature is 28 °C) and a temperature factor obtained from Hanson et al. (2011). As described in Lauerwald et al. (2017), besides CO_2 originated from fluvial DOC, "dissolved CO_2 inputs from the decomposition from flooded SOC and litter are also added at the time step of 6 minutes to represent the continuous additions of CO_2 during the water–atmosphere gas exchange. For each time step, the CO_2 partial pressures (pCO_2) in the water column is calculated from the concentration of dissolved CO_2 and the temperature-dependent solubility of CO_2 (Telmer and Veizer, 1999). The CO_2 evasion is finally calculated based on the water–air gradient in pCO_2, the gas exchange velocity and the surface water area available for gas exchange" (p. 3835). In addition, swamp and wetland are also represented in the routing scheme of ORCHILEAK. More detailed descriptions can be found in Lauerwald et al. (2017).

2.1.2 Sediment and carbon delivery from upland soil to river network

Using an upscaling scheme, the erosion-induced sediment and POC delivery from upland soil to river network, as well as the dynamics of vertical SOC distribution due to soil erosion had already been implemented in ORCHIDEE-MUSLE (Zhang et al., 2020). The sediment delivery from small headwater basins to river network (i.e. gross upland soil erosion – sediment deposition within headwater basins) is simulated using the Modified Universal Soil Loss Equation model (MUSLE, Williams, 1975). For the upscaling, MUSLE is first applied to high-resolution (3″) topographic and soil erodibility data. As introduced in Zhang et al. (2020), "the

https://doi.org/10.5194/esd-2022-4
Preprint. Discussion started: 1 February 2022


Earth System Dynamics Discussions Open Access EGU

daily sediment delivery rate from each headwater basin (S_{i_ref}, Mg day^{-1} basin^{-1}) is first calculated for a given set of reference runoff and vegetation cover conditions:

$$S_{i_{ref}} = a\left(Q_{i_{ref}} q_{i_{ref}}\right)^{b} K_i LS_i C_{ref} P_{ref} \quad (1)$$

where Q_{i_ref} is the total water discharge (m^3 day^{-1}) at the outlet of headwater basin i for the daily reference runoff condition (R_{ref}) of 10 mm day^{-1}. In Eq. 1, q_{i_ref} is the daily peak flow rate (m^3 s^{-1}) at the headwater basin outlet under the assumed reference runoff condition. Similar to the SWAT model (Soil and Water Assessment Tool, Neitsch et al., 2011), q_{i_ref} was calculated from the reference maximum 30-minutes runoff (= 1 mm 30-minutes^{-1}) depth and drainage area according to the following equation:

$$q_{i\_ref} = \frac{R_{30\_ref}}{30\times 60}\left(DA_i^{(d\, DA_i^{c})}\right) 1000 \quad (2)$$

where R_{30_ref} (= 1 mm 30-minutes^{-1}) is the assumed daily maximum 30-minutes runoff" (p. 5-6). The coefficients a and b in Eq. 1 and c and d in Eq. 2 need to be calibrated (see section 2.3 and Table A1). In Eq. 1, the term LS_i is the combined dimensionless slope length and steepness factor calculated based on the DA_i and the average slope steepness (extracted from DEM) of headwater basin i (Moore and Wilson, 1992). C_{ref} (0-1, dimensionless) in Eq. 1 represents the cover management factor and is set to 0.1 for the reference state. The soil erodibility factor K_i (Mg MJ^{-1} mm^{-1}) is calculated using the method of the EPIC model (Sharpley and Williams, 1990) based on SOC and soil texture data obtained from the GSDE database (Table 1). The term P_{ref} (0-1, dimensionless) in Eq. 1 is a factor representing erosion control practices. It was set to 1, as we did not consider the impacts of soil conservation practices in reducing soil erosion rate. Note that it does not matter which value is chosen for the R_{ref}, R_{30_ref}, C_{ref} and P_{ref} as long as they are used consistently throughout a study.

For the use of these reference sediment delivery estimates in ORCHILEAK Clateral, the values were first calculated for each headwater basin derived from high resolution geodata, then aggregated to 0.5° grid cells – the scale used in our simulations and required to maintain computational efficiency (also limited by the availability of climate and land cover forcing data).

This aggregated dataset is then used to force the simulation of Then, the actual daily sediment delivery (S_{iday}, g day^{-1} grid^{-1}) in ORCHIDEE Clateralis calculated, by comparing the simply

https://doi.org/10.5194/esd-2022-4
Preprint. Discussion started: 1 February 2022


Earth System Dynamics Discussions

based on the estimated reference sediment delivery rates of Eq. (1) and on the ratios between actual runoff and land cover conditions to and the assumed reference conditions used to create that forcing file (Eq. 4).

$$S_{ref} = \sum_{i=1}^{n}(S_{i\_ref}) \times 10^6 \quad (3)$$

$$S_{iday}=S_{ref}\left(\frac{R_{iday}\,R_{30\_iday}}{R_{ref}\;R_{30\_ref}}\right)^{b}\frac{C_{iday}}{C_{ref}} \quad (4)$$

where R_{iday} (mm day^{-1}) is the daily total surface runoff simulated by the hydrological module or ORCHIDEE-MUSLE at 0.5° spatial resolution every 30 minutes. R_{30_k} (mm 30-min^{-1}) is the maximum value of the 48 half-hour runoffs in each day. C_{iday} (0-1, unitless) is the daily actual cover management factor, calculated based on the fraction of surface vegetation cover, the amount of litter carbon and the biomass of living roots in each PFT within each 0.5°×0.5° grid cell. R_{ref}, R_{30_ref}, C_{ref} and P_{ref} are the reference values used to estimate the reference sediment delivery rates as describe above.

Daily POC delivery to river headstream in each 0.5° grid cell is finally simulated based on the sediment delivery rate and the average SOC concentration of surface soil layers (0-20 cm). The vertical SOC profile is updated every day based on the average depth of eroded soil for each PFT in each 0.5° grid cell of ORCHIDEE. For more detailed description of the ORCHIDEE-MUSLE, we refer to Zhang et al. (2020).

2.2 Sediment and POC transport in inland water network

Through the merge of the model branches ORCHILEAK and ORCHIDEE-MUSLE, the new branch ORCHIDEE-$C_{lateral}$ combines the novel features of both sources (DOC and POC) described above. The development of ORCHIDEE-$C_{lateral}$ is complemented by a representation of the sediment and POC transport through the river network that is completely novel and described below.

2.2.1 Sediment transport

https://doi.org/10.5194/esd-2022-4
Preprint. Discussion started: 1 February 2022

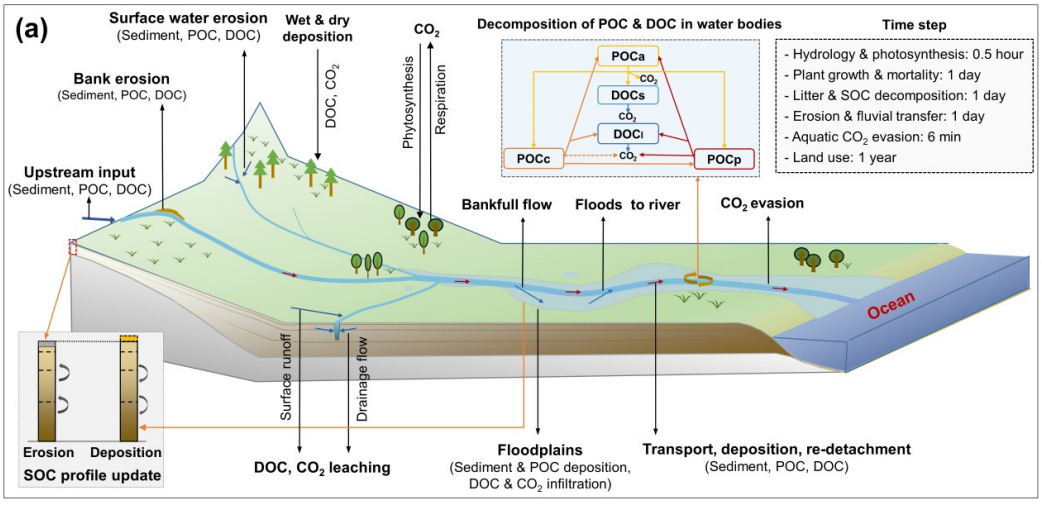

Figure 1 Simulated lateral transfer processes of water, sediment and carbon (POC, DOC and CO_2) in ORCHIDEE-$C_{lateral}$ (a) and a schematic plot for the reservoirs and flows of water, sediment and carbon represented in the routing module of ORCHIDEE-$C_{lateral}$. S_{soil} is the soil pool. S_{rivbed} is the sediment (also POC) deposited in river bed. S_{fast}, S_{slow}, S_{river} and S_{flood} are the 'fast', 'slow', stream and flooding water reservoir, respectively. F_{RO} and F_{DR} are the surface runoff and belowground drainage, respectively. F_{Fout} and F_{Sout} are the flows from fast and slow reservoir to the stream reservoir, respectively. F_{up2riv} and F_{up2fld} are the inputs from upstream basins to the stream reservoir and flooding reservoir of the target basin, respectively. $F_{dow2riv}$ and

https://doi.org/10.5194/esd-2022-4
Preprint. Discussion started: 1 February 2022


Earth System Dynamics Discussions Open Access EGU

290 $F_{down2fld}$ are the outputs from the stream reservoir of the target basin to the stream reservoir and
291 flooding reservoir of the neighbouring downstream basin, respectively. $F_{fld2riv}$ is the return flow
292 from flooding reservoir to stream reservoir. $F_{bed2fld}$ is the transform from deposited sediment in
293 river bed to floodplain soil. F_{bero} is bank erosion. F_{rd} and F_{rero} are the deposition and re-
294 detachment of sediment and POC in river channel, respectively. F_{sub} is the flux of DOC and CO2
295 from floodplain soil (originated from the decomposition of submerged litter and soil carbon) to
296 the overlying flooding water. F_{fd} is the deposition of sediment and POC and the infiltration of
297 water and DOC. F_D is the wet and dry deposition of DOC from atmosphere and plant canopy.

298

299 Simulation of sediment transport through the river network basically follows the routing scheme
300 of surface water and DOC of ORCHILEAK (Fig. 1). Along with surface runoff (F_{RO_h2o}, m^3 day^{-1}),
301 the sediment delivery (F_{RO_sed}, g day^{-1}) from uplands in each basin (i.e. each 0.5° grid in the
302 case of this study) initially feeds an aboveground water reservoir with a so-called fast water
303 residence time (S_{fast_h2o}, m^3). From this fast water reservoir, a delayed outflow feeds into the so-
304 called stream reservoir (S_{riv}, m^3, Fig. 1b). Daily water (F_{Fout_h2o}, m^3 day^{-1}) and sediment (F_{Fout_sed},
305 g day^{-1}) flows from fast water reservoir to stream reservoir are calculated from a basin-specific
306 topographic index f_{topo} (unitless,) extracted from a forcing file (Table 1) and a reservoir-specific
307 factor τ which translates f_{topo} into a water residence time of each reservoir (Eqs. 5, 6). Following
308 Guimberteau et al. (2012), the τ of the fast water reservoir (τ_{fast}) is set to 3.0 days. As the
309 sediment delivery calculated from MUSLE is the net soil loss from headwater basins (gross soil
310 erosion – soil deposition within headwater basins), we assumed that there is no sediment
311 deposition in the fast reservoir, and that all of the sediment in the fast reservoir enter into stream
312 reservoir. In addition, only the surface runoff causes soil erosion. The belowground drainage
313 (F_{DR_h2o}, m^3 day^{-1}) only transport DOC and dissolved CO_2 to the stream reservoir (Fig. 1b).

314 $$F_{Fout\_h2o} = \frac{S_{fast\_h2o}}{\tau_{fast}\, f_{topo}} \quad (5)$$

315 $$F_{Fout\_sed} = \frac{S_{fast\_sed}}{\tau_{fast}\, f_{topo}} \quad (6)$$

316 The budget of the suspended sediment in stream reservoir (S_{riv_sed}, g) is determined by the
317 F_{Fout_sed}, upstream sediment input (F_{up2riv_sed}, g day^{-1}), the sediment input in flooding water
318 returning to the river ($F_{fld2riv\_sed}$, g day^{-1}), re-detachment of the previously deposited sediment in
319 the river bed (F_{rero_sed}, g day^{-1}), bank erosion (F_{bero_sed}, g day^{-1}), sediment deposition in the river

https://doi.org/10.5194/esd-2022-4
Preprint. Discussion started: 1 February 2022


Earth System Dynamics Discussions

bed (F_{rd_sed}, g day^{-1}) and sediment transported to downstream river stretches ($F_{down2riv\_sed}$, g day^{-1}) and, occasionally, floodplains ($F_{down2fld\_sed}$, g day^{-1}) (Eq. 7).

$$\frac{dS_{riv\_sed}}{dt} = F_{Fout\_sed} + F_{up2riv\_sed} + F_{fld2riv\_sed} + F_{rero\_sed} + F_{bero\_sed} - F_{rd\_sed} - F_{down2riv\_sed} - F_{down2fld\_sed} \quad (7)$$

Sediment transport capacity (TC, g m^{-3}), defined as the maximum load of sediment that a given flow rate can carry, determines the amount of suspended sediment that can be transported to the downstream grid cell (e.g. $F_{down2riv\_sed}$, $F_{down2fld\_sed}$), as well as the amount of suspended sediment that will deposit on the river bed (F_{rd_sed}) or the erosion rate of the river bed (F_{rero_sed}) or river bank (F_{bero_sed}) (Arnold et al., 1995; Nearing et al., 1989; Neitsch et al., 2011). Several physics-based algorithms have been proposed to accurately calculate the TC of stream flows (Arnold et al., 1995; Molinas and Wu, 2001; Nearing et al., 1989). These algorithms mostly require detailed information about the stream power (e.g. flow speed and depth), geomorphic properties of the river channel (e.g. slope and hydraulic radius) and the physical properties of the sediment particles (e.g. median grain size) (Neitsch et al., 2011). They are good predictors to estimate TC in rivers with detailed observation data on local stream, soil, geomorphic properties. Unfortunately, it is not practical to implement those algorithms in ORCHIDEE-$C_{lateral}$ due to the lack of appropriate forcing data at large scale as well as the relatively rough representation of stream flow dynamics compared to hydrological models for small basins. For example, runoff and sediment from all headwater basins in one 0.5° grid cell of ORCHIDEE-$C_{lateral}$ are assumed to flow into one single virtual river channel. Although the total river surface area in each grid cell is represented (obtained from forcing file (Table 1), Lauerwald et al., 2015), the length, width and depth of the river channel are unknown. Furthermore, in reality, there can be multiple river channels in the area represented by each grid cell, and these channels might flow to different directions. This illustrates the difficulty to simulate the detailed hydraulic dynamics of the stream flow in each grid.

We also noticed that previous studies have derived empirical functions of upstream drainage area (e.g. Luo et al., 2017) or upstream runoff (e.g. Yamazaki et al., 2011) to calculate the river width and depth, allowing to simulate the water flow in the river channel using physically-based algorithms. Unfortunately, to obtain a good fit of the simulated river discharges against observations, the parameters in the empirical functions for calculating river width and depth generally need to be calibrated separately for each catchment (Luo et al., 2017), an approach that

https://doi.org/10.5194/esd-2022-4
Preprint. Discussion started: 1 February 2022


Earth System Dynamics Discussions

is incompatible with large-scale simulations like those performed here. Without such calibration, the simulated geometrical properties of the river channel and runoff are prone to large uncertainties, thus rendering the simulation of sediment transport at continental or global scale using physically-based algorithms a more challenging task.

In this study, we used an empirical equation adapted from the WBMsed model, which has been proven effective in simulating the suspended sediment discharges in global large rivers (Cohen et al., 2014), to estimate the TC (g m^{-3}) of stream flow:

$$TC = \frac{\omega\, {q_{ave}}^{0.3}\, A^{0.5} \left(\frac{q_{iday}}{q_{ave}}\right)^{e_1} (24\times60\times60)}{F_{down2riv\_h2o}} \quad (8)$$

$$e_1 = 1.5 - max(0.8, 0.145 \log_{10} A) \quad (9)$$

where ω is the coefficient of proportionality, q_{ave} (m^3 s^{-1}) is long-term average stream flow rate obtained from an historical simulation by ORCHILEAK (Table 1), q_{iday} (m^3 s^{-1}) is stream flow rate on day i, A (m^2) is the upstream drainage area, $F_{down2riv\_sed}$ (m^3 day^{-1}) is the daily downstream water discharge from the stream reservoir. In the stream reservoir of each basin, net deposition occurs when TC is smaller than the concentration of suspended sediment, and the daily deposited sediment (F_{rd_sed}, g day^{-1}) is calculated based on the surplus of the suspended sediment:

$$F_{rd\_sed} = c_{rivdep}\left(S_{riv\_sed} - TC\, S_{riv\_h2o}\right) \quad (10)$$

where c_{rivdep} (0-1, unitless) is the daily deposited fraction of the sediment surplus. Net erosion of the previously deposited sediment in river bed (S_{rivbed_sed}, Fig. 1) or the river bank occurs when TC is larger than the concentration of suspended sediment. We assumed that the erosion of river bank occurs only after all of the S_{rivbed_sed} has been eroded. Thus the daily erosion rate (F_{rero_sed}, g day^{-1}) in river channel is calculated as:

$$F_{rero\_sed} = \begin{cases} c_{ebed}\left(TC\, S_{riv\_h2o} - S_{riv\_sed}\right), & c_{ebed}\left(TC\, S_{riv\_h2o} - S_{riv\_sed}\right) \le S_{rivbed\_sed} \\ S_{rivbed\_sed} + c_{ebank}\left(TC\, S_{riv\_h2o} - S_{riv\_sed} - S_{rivbed\_sed}\right), & c_{ebed}\left(TC\, S_{riv\_h2o} - S_{riv\_sed}\right) > S_{rivbed\_sed} \end{cases} \quad (11)$$

where c_{ebed} (0-1, unitless) and c_{ebank} (0-1, unitless) are the fraction of sediment deficit that can be complemented by erosion of river bed and bank, respectively. After updating the S_{riv_sed} based on the F_{rd_sed} or F_{rero_sed}, the sediment discharge to downstream basin ($F_{down2riv\_sed}$, g day^{-1}) is calculated based on the ratio of downstream water discharge to the total stream reservoir:

$$F_{down2riv\_sed} = \left(S_{riv\_sed} - F_{rd\_sed} + F_{rero\_sed}\right) \frac{F_{down2riv\_h2o}}{S_{riv\_sh2o}} \quad (12)$$

https://doi.org/10.5194/esd-2022-4
Preprint. Discussion started: 1 February 2022


Earth System Dynamics Discussions

In each basin, the bankfull flow occurs when S_{riv_h2o} exceeds the maximum water storage of river channel (S_{rivmax}, g), which is defined by a forcing file (Table 1). Sediment flow from stream to floodplain ($F_{down2fld\_sed}$, g day^{-1}) follows the flooding water, and it is calculated as:

$$F_{down2fld\_sed} = \left(S_{riv\_sed} - F_{rd\_sed} + F_{rero\_sed}\right)\frac{F_{down2fld\_h2o}}{S_{riv\_sh2o}} \quad (13)$$

$$F_{down2fld\_h2o} = \left(S_{riv\_h2o} - F_{down2riv\_h2o} - S_{rivmax}\right)\frac{f_{A\_fld}}{f_{A\_fld}+f_{A\_riv}} \quad (14)$$

where f_{A_fld} (0-1, unitless) and f_{A_riv} (0-1, unitless) is the fraction of floodplain area and river surface area in each basin, respectively. Following the routing scheme of ORCHILEAK, the bankfull flow of a specific basin is assumed to enter the floodplain in the neighbouring downstream basin instead of the basin where it originates.

The sediment balance in flooding reservoir (S_{fld_sed}, g) is controlled by sediment input from the upstream basins (F_{up2fld_sed}, g day^{-1}), the sediment flowing back to the stream reservoir ($F_{fld2riv\_sed}$, g day^{-1}) and the sediment deposition (F_{fd_sed}, g day^{-1}) (Fig. 1):

$$\frac{dS_{fld\_sed}}{dt} = F_{up2fld\_sed} - F_{fld2riv\_sed} - F_{fd\_sed} \quad (15)$$

Sediment deposition in flooding water is calculated as the sum of a natural deposition and the deposition due to evaporation (E_{h2o}, m^3 day^{-1}) and infiltration (I_{h2o}, m^3 day^{-1}) of the flooding waters:

$$F_{fd\_sed} = c_{flddep}\, S_{fld\_sed} - S_{fld\_sed}\frac{E_{h2o}+I_{h2o}}{S_{fld\_h2o}} \quad (16)$$

where c_{flddep} (0-1, unitless) is the daily deposited fraction of the suspended sediment in flooding waters. After removing the deposited sediment from S_{fld_sed}, $F_{fld2riv\_sed}$ is calculated based on the ratio of ratio of $F_{fld2riv\_h2o}$ to the total flooding reservoir:

$$F_{fld2riv\_sed} = S_{fld\_sed}\frac{F_{fld2riv\_h2o}}{S_{fld\_h2o} - E_{h2o} - I_{h2o}} \quad (17)$$

$$F_{fld2riv\_h2o} = \frac{S_{fld\_h2o} - E_{h2o} - I_{h2o}}{\tau_{flood}\, f_{topo}} \quad (18)$$

where τ_{flood} is a factor which translates f_{topo} into a water residence time of the flooding reservoir. Same to ORCHILEAK, it is set to 1.4 (day m^{-2}) in this study.

Note that as the upland soil in ORCHIDEE is composed of clay, silt and sand particles, so that the dynamics of clay-, silt- and sand-sediment in inland waters are simulated separately. To represent the selective transport of clay-, silt- and sand-sediment, the model parameter ω (Eq. 8)

https://doi.org/10.5194/esd-2022-4
Preprint. Discussion started: 1 February 2022


Earth System Dynamics Discussions Open Access EGU

and c_{rivdep} (Eq. 10) are set to different values when calculating the sediment transport capacity and the deposition of surplus suspended sediment for different particle sizes (Table A1).

2.2.2 POC transport and decomposition

Many studies described the selective transport of POC and sediment of different particles sizes. The enrichment ratio (defined as the ratios of fraction of any given component in the transported sediment to that in the eroded soils) of POC in the transported sediment generally showed significant positive correlation to the fine sediment particles (e.g. fine silt and clay), but negative correlation to the coarse sediment particles (Galy et al., 2008; Haregeweyn et al., 2008; Nadeu et al., 2011; Nie et al., 2015). In ORCHIDEE-$C_{lateral}$, the physical movements of POC in inland water systems are simply assumed to follow the flows of finest clay-sediment (Fig. 1b). For example, the fractions of riverine suspended POC which is deposited on the river bed (F_{rd_POC}, g C day^{-1}) or is transported to the river channel ($F_{down2riv\_POC}$, g C day^{-1}) or floodplain ($F_{down2fld\_POC}$, g C day^{-1}) of the downstream grid cell are assumed to be equal to the corresponding fractions of clay-sediment (Eqs. 19-21). Also flows of suspended POC in flooding waters to floodplain soil (F_{fd_POC}, g C day^{-1}) or back to the stream reservoir ($F_{fld2riv\_POC}$, g C day^{-1}), as well as the resuspension of POC from the river bed (F_{rero_POC}, g C day^{-1}) are scaled to the simulated flows of clay-sediment (Eqs. 22-24). Note that, similar to SOC, the POC in aquatic reservoirs are divided into three pools: the active (POC_a), slow (POC_s) and passive pool (POC_p) (Fig. 1a). The eroded active, slow and passive SOC flow into the corresponding POC pools in the 'fast' water reservoir (Fig. 1b).

$$F_{rd\_POC} = S_{riv\_POC}\frac{F_{rd\_sed\_clay}}{S_{riv\_sed\_clay}} \quad (19)$$

$$F_{down2riv\_POC} = S_{riv\_POC}\frac{F_{down2riv\_sed\_clay}}{S_{riv\_sed\_clay}} \quad (20)$$

$$F_{down2fld\_POC} = S_{riv\_POC}\frac{F_{down2fld\_sed\_clay}}{S_{riv\_sed\_clay}} \quad (21)$$

$$F_{fd\_POC} = S_{fld\_POC}\frac{F_{fd\_sed\_clay}}{S_{fld\_sed\_clay}} \quad (22)$$

$$F_{fld2riv\_POC} = S_{fld\_POC}\frac{F_{fld2riv\_sed\_clay}}{S_{fld\_sed\_clay}} \quad (23)$$

$$F_{bed2fld\_POC} = S_{rivbed\_POC}\frac{F_{bed2fld\_sed}}{S_{rivbed\_sed}} \quad (24)$$

https://doi.org/10.5194/esd-2022-4
Preprint. Discussion started: 1 February 2022


Earth System Dynamics Discussions

The representation of POC dynamics in the aquatic reservoirs and bed sediment involve as well decomposition, which follows largely the scheme used for SOC (Fig. 1a). However, instead of using the rate modifiers for soil temperature and moisture used in the soil carbon module, daily decomposition rates (F_{POC_i}, g C day^{-1}) of each POC pool (S_{POC_i}, g C) are simulated to vary with water temperature based on the Arrhenius term which is used to simulate the DOC decomposition in ORCHILEAK (Hanson et al., 2011; Lauerwald et al., 2017):

$$F_{POC\_i} = S_{POC\_i} \frac{1.073^{(T_{water}-28.0)}}{\tau_{poc\_i}} \quad (25)$$

where T_{water} (°C) is the temperature of water reservoirs. For the POC stored in bed sediment, temperature of the stream reservoir is used to calculate the decomposition rate. τ_{POC_i} is the turnover time of the *i* (active, slow and passive) POC pool. We assumed that the base turnover times of active (0.3 year) and slow (1.12 years) POC pools are the same as for the corresponding SOC pools. The passive SOC pool is generally regarded as the SOC which is associated to soil minerals or enclosed in soil aggregates (Parton et al., 1987). During the soil erosion and sediment transport processes, the aggregates break down and the passive POC loses its physical protection from decomposition (Chaplot et al., 2005; Hu and Kuhn, 2016; Polyakov and Lal, 2008; Wang et al., 2014a). To represent the acceleration of passive POC decomposition due to aggregate breakdown, we assume that the turnover time of the passive POC is same to the active POC (0.3 year), rather than the passive SOC (462 years). Similar to the scheme used to simulate SOC decomposition in ORCHILEAK, the decomposed POC from each of the active, slow and passive pool flows to other POC pools, to DOC pools or is released to the atmosphere as CO_2 (Fig. 1). Fractions of the decomposed POC flowing to different POC and DOC pools or to the atmosphere are set to the same values used in ORCHILEAK for simulating the fates of the decomposed SOC pools.

Changes in the vertical SOC profile of floodplain soils following sediment deposition is simulated at the end of every daily modelling time-step, after physical transfers and decomposition of POC have been calculated. The sediment deposited on the floodplain becomes the new surface soil layer, and the active, slow and passive POC flow into the active, slow and passive SOC pools in surface soil layer, respectively. SOC in the original surface and subsurface soil layers is transferred sequentially to the adjacent deeper soil layers. As the vertical soil profile in ORCHILEAK is described by an 11-layer discretization of a 2 m soil column, we introduce a deep (> 2 m) soil pool (S_{deep}) to represent the soil and carbon transferred down from the 11th soil

https://doi.org/10.5194/esd-2022-4
Preprint. Discussion started: 1 February 2022


Earth System Dynamics Discussions

462 layer following ongoing floodplain deposition. Decomposition rates of the organic carbon in this
463 deep soil pool are assumed to be same to those in the 11th (deepest) soil layer. Note that when
464 the soil erosion rate of the floodplain soil is larger than the sediment deposition rate, sediment
465 and organic carbon in S_{deep} move up to replenish the stocks of the 11th soil layer.

466 **2.3 Model application and evaluation**

467 In this study, the ORCHIDEE-$C_{lateral}$ was applied over Europe (-30W– 70E, 34N-75N, also
468 includes a part of Middle East and Africa, Fig. S1 in the Supplement), where extensive
469 observation datasets are available to calibrate and evaluate our model (Table 1). The return
470 period of daily bankfull flow ($P_{flooding}$, year), which represents the average interval between two
471 flooding days and is used in this study to produce the forcing file of S_{rivmax} from a pre-run of
472 ORCHILEAK. Note that $P_{flooding}$ is generally shorter than the return period of real flooding
473 events, as the flooding may occur in several continuous days and the all flooding waters
474 occurring on these continuous days are generally regarded to belong to the same flooding event
475 (Fig. S1). $P_{flooding}$ shows substantial spatial variations following climate and topography
476 (Schneider *et al*., 2011). In this study, we assumed that $P_{flooding}$ for all rivers in Europe are the
477 same and the observed long-term (1961–2000) average bank full flow rate ($m^3\ s^{-1}$) at 66 sites
478 obtained from Schneider *et al*. (2011) was used to calibrate $P_{flooding}$ (= 0.1 year, Table A1). Same
479 to Zhang et al. (2020), the parameters *a*, *b*, *c* and *d* in Eq. 1 and 2 (Table A1) were calibrated at
480 57 European catchments (Fig. S2d) against the modelled sediment delivery data obtained from
481 the European Soil Data Centre (ESDAC, Borrelli et al., 2018). The sediment delivery data from
482 the ESDAC product is simulated by the WaTEM/SEDEM model using high-resolution data of
483 topography, soil erodibility, land cover and rainfall. It has been calibrated and validated using
484 observed sediment fluxes from 24 European catchments (Borrelli et al., 2018).

485 Parameters controlling sediment transport, deposition and re-detachment (i.e. ω, c_{rivdep}, c_{flddep},
486 c_{ebed} and c_{ebank}, Table S1) in stream and flooding reservoirs were calibrated against the observed
487 long-term averaged sediment discharge rate (Table 1). We also conducted a sensitivity analysis
488 to test the sensitivity of the simulated riverine sediment and carbon discharges to these
489 parameters, following the method used in Tian et al. (2015). The sensitivity of simulation results
490 was evaluated based on the relative changes in simulated riverine sediment and carbon
491 discharges to a 10% increase and decrease of each parameter (Table S1). Result of the sensitivity

https://doi.org/10.5194/esd-2022-4
Preprint. Discussion started: 1 February 2022

analysis shows that the simulated riverine sediment and POC discharges are most sensitive to c_{rivdep} in Eq. 5, followed by ω in Eq. 8 (Fig. S3). Compared to c_{rivdep} and ω, the simulated riverine sediment and POC discharges are less sensitive to c_{flddep}, c_{ebed} and c_{ebank}. With 10% changes in c_{flddep}, c_{ebed} or c_{ebank}, the changes in riverine sediment and POC discharges are generally less than 3%. In addition, the changes in simulated riverine DOC and CO_2 discharges are mostly less than 1% with 10% changes in ω, c_{flddep}, c_{ebed} and c_{ebank}. Nonetheless, a 10% change in c_{rivdep} can lead to a change of about 5% in the simulated riverine CO_2 discharge (Fig. S3).

After parameter calibration, ORCHIDEE-$C_{lateral}$ was applied to simulate the lateral transfers of water, sediment and organic carbon in European rivers over the period 1901-2014. Before this historical simulation, ORCHIDEE-$C_{lateral}$ was run over 10,000 years (spin-up) until the soil carbon pools reached a steady state. In the 'spin-up' simulation, the PFT maps, atmospheric CO_2 concentrations and meteorological data during 1901–1910 were used repeatedly as the forcing data. The finally simulated water discharge rates in European rivers were evaluated using observation data at 93 gauging sites (Fig. S2a) from the Global Runoff Data Base (GRDC, Table 1). The simulated bankfull flows were evaluated against observed long-term (1961–2000) average bankfull flows at 66 sites (Fig. S2b) from Schneider *et al*. (2011). The simulated riverine sediment discharge rate is evaluated using observation data from the European Environment Agency and existing publications (see Table 1) at 221 gauging sites (Fig. S2c). The riverine total organic carbon (TOC), POC and DOC concentrations provided by the GLObal RIver Chemistry Database (GLORICH, Hartmann et al., 2019) at 346 sites (Fig. S2d) were used to evaluate the simulated riverine POC and DOC concentrations. Note that observations in the GLORICH database which are measured at gauging sites with drainage area $<1.0\times10^4$ km^2 were excluded from our model evaluation, because these small catchments cannot be represented by the coarse river network scheme at 0.5 degree (ca. 55 km at the equator). Among the retained 346 gauging sites, TOC concentrations were measured at 188 sites, DOC was measured at 314 sites. POC was measured at only 3 sites in the Rhine catchment.

3 Results and Discussion

3.1 Model evaluation

3.1.1 Stream water discharge and bankfull flow

https://doi.org/10.5194/esd-2022-4
Preprint. Discussion started: 1 February 2022


Earth System Dynamics Discussions Open Access EGU

Evaluation of our simulation results using *in situ* observation data from Europe rivers indicates that ORCHIDEE-$C_{lateral}$ well reproduces the magnitude and interannual variation of water discharge rates in major European rivers (Figs. 2a and S4). Overall, the simulated riverine water discharge rate explained 94% (Fig. 2a) of the spatial variation of the observed long-term average water discharge rates across 93 gauging sites in Europe (Fig. S2a). Relative biases (calculated as: $\frac{simulation-observation}{observation} \times 100\%$, as used through the manuscript if not otherwise stated) of the simulated average water discharge rates compared to the observations are mostly smaller than 30% (Fig. 2a). For major European rivers, such as the Rhine, Danube, Elbe, Rhone and Volga, ORCHIDEE-$C_{lateral}$ also captures the interannual variation of the water discharge rate (Fig. S4). We recognize that ORCHIDEE-$C_{lateral}$ may overestimate or underestimate the water discharge rate in some rivers (Fig. 2a), particularly in smaller rivers where discrepancy between the stream routing scheme (delineation of catchment boundaries) extracted from the forcing data at 0.5° resolution and the real river network (Fig. S5) can be substantial. An over- or underestimation of the catchment area by the forcing data will introduce a proportional bias to the average amount of simulated discharge from that catchment. Another problem are stream channel bifurcations which occur in reality, but which are not represented in a stream network derived from a digital elevation model. For example, in the Danube river delta, a fraction of the discharge is actually exported to the sea through the Saint George Branch, in addition to the water discharge through the main river channel (Fig. S5b). This explains why the simulated water discharge rate at the outlet of Danube catchment is larger than the observation at the Ceatal, Romania (identify number in the GRDC database is 6742900, Fig. S4m), where only the main stream discharge was measured.

https://doi.org/10.5194/esd-2022-4
Preprint. Discussion started: 1 February 2022

Earth System Dynamics
Discussions
Open Access
EGU

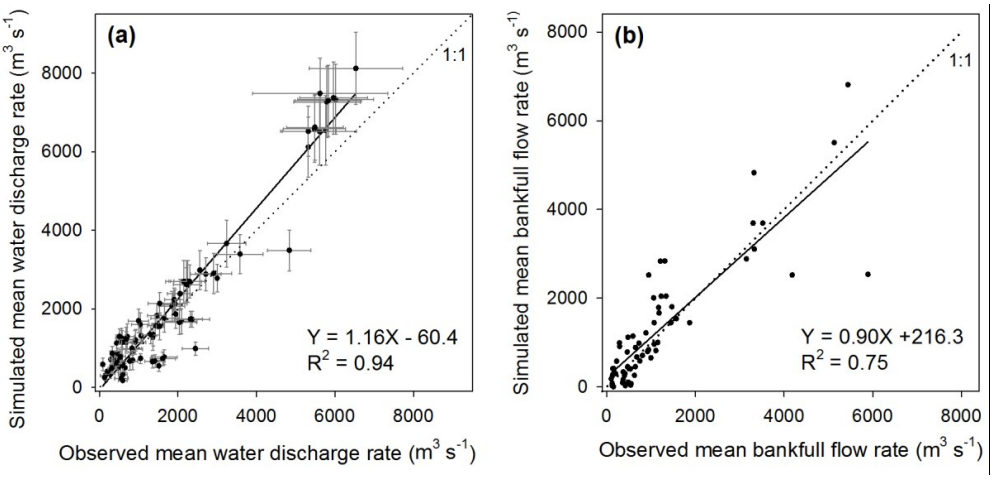

543

544 **Figure 2** Comparison between observed and simulated riverine water discharge rates (a) and
545 bankfull flow rates (b). In figure (a), the error bar denotes the standard deviation of interannual
546 variation. Sources of the observed riverine water discharge rate and bankfull flow rate can be
547 found in Table 1.

548

549 By setting the return period of the daily flooding rate to 0.1 year, the simulated bankfull flow
550 rates compare well to observations at the 66 sites for which data was available (Fig. 2b). Overall,
551 the simulation result explained 75% of the inter-site variation of the observed bankfull flow
552 rates. Relative biases of the simulated bankfull flow rates are generally lower than 30%, although
553 the relative bias may be larger than 100% at some sites.

554 **3.1.2 Sediment transport**

555 The simulated area-averaged sediment delivery rates from upland to river network by the
556 ORCHIDEE-$C_{lateral}$ are overall comparable to those simulated by the WaTEM/SEDEM for most
557 catchments in Europe (Figs. 3a and S2d). In the two catchments in the Apennine Peninsula,
558 ORCHIDEE-$C_{lateral}$ gives a drastically lower estimation on the sediment delivery rates compared
559 to WaTEM/SEDEM. By excluding these two catchments, ORCHIDEE-$C_{lateral}$ reproduces 72% of
560 the spatial variation of the sediment delivery rates estimated by the WaTEM/SEDEM (Fig. 3a).

561 ORCHIDEE-$C_{lateral}$ reproduces 83% of the inter-site variation of the sediment discharge rates
562 across Europe (Fig. 3b). Simulation of the riverine sediment discharge rate at large spatial scale

https://doi.org/10.5194/esd-2022-4
Preprint. Discussion started: 1 February 2022

Earth System Dynamics
Discussions
Open Access
EGU

563 is still a big challenge. It generally needs detailed information on the stream flow, geomorphic
564 properties of river channel and the particle composition of the suspended sediment (Neitsch et
565 al., 2011). Moreover, the parameters of existing sediment transport models usually require
566 recalibration when they are applied to different catchments (Gassman et al., 2014; Oeurng et al.,
567 2011; Vigiak et al., 2017). In ORCHIDEE-$C_{lateral}$, the sediment processes in river networks are
568 simulated using simple empirical functions and parameters based on a routing scheme at a spatial
569 resolution of 0.5° (section 2.2.1). Detailed information about the stream flow (e.g. cross-
570 sectional area) and the geomorphic properties of river channels are not represented. Sediment
571 discharge in all catchments was simulated using a universal parameter set. This may explain why
572 ORCHIDEE-$C_{lateral}$ fails to capture the sediment discharge rates in some specific catchments,
573 especially those with relatively small drainage areas (e.g. < 5×10^3 km^2).

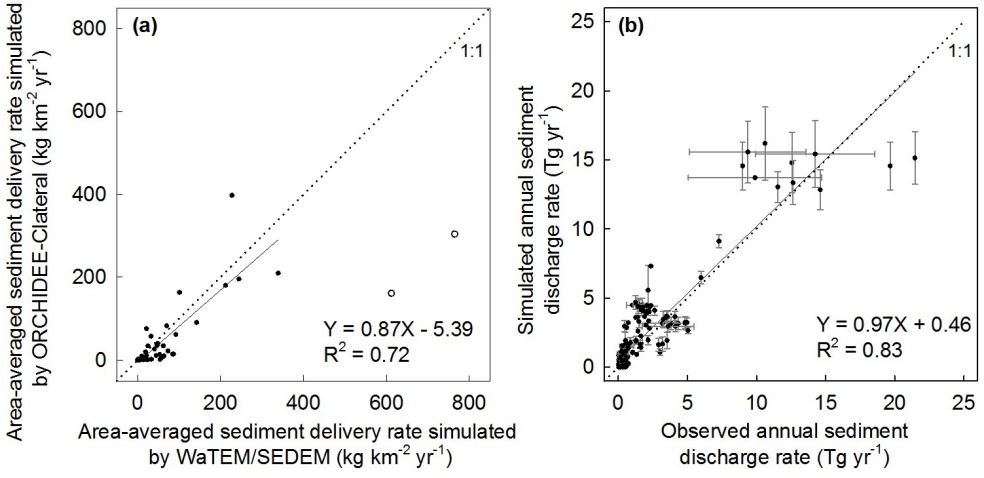

574

575 **Figure 3** Comparison between the simulated area-averaged sediment delivery rate from uplands
576 to river network from ORCHIDEE-$C_{lateral}$ and WaTEM/SEDEM (a), and the comparison between
577 observed and simulated annual sediment discharge rates at 221 gauging sites (b). In figure (a),
578 the two hollow dots represent the sediment delivery rates at the two catchments in the Apennine
579 Peninsula (Fig. S1d). The regression function in figure (a) was obtained based on the values of
580 all solid dots, excluding the two hollow dots. In figure (b), the error bar denotes the standard
581 deviation of interannual variation. Sources of the observed annual sediment discharge rate in
582 Table 1.

583

https://doi.org/10.5194/esd-2022-4
Preprint. Discussion started: 1 February 2022


Earth System Dynamics Discussions

584 **3.1.3 Organic carbon transport**

585 Simulation of the riverine carbon discharge rate at large spatial scale is even a bigger challenge
586 than simulating sediment discharge, as the riverine carbon discharge is controlled by many
587 factors, such as upland topsoil SOC concentrations, soil erosion rate, transport and deposition
588 rate of clay fraction in river channel and on floodplain, and the decomposition of POC in transit
589 and in aquatic sediments. As described above, the simulated water discharge rate, bankfull flow
590 and sediment discharge rate are overall comparable to observation (Figs. 2 and 3). The simulated
591 total SOC stock in the top 0-30 cm soil layer in Europe of 107 Pg C is close to the value
592 extracted from the HWSD database (106 Pg C), but significantly lower than the values extracted
593 from some other databases, such as the GSDE (249 Pg C), SoilGrids (202 Pg C), S2017 (148 Pg
594 C) and landGIS (226 Pg C) (Fig. S6a). Distribution of the simulated SOC stock along the latitude
595 gradients (30° N – 75° N) are overall comparable to those extracted from the HWSD and S2017
596 databases (Fig. S6). But even compared to these two databases, our model still underestimated
597 the SOC stock in southern Europe (30° N – 41° N).

598 Comparison of the simulated concentrations of riverine organic carbon and the observations
599 obtained from the GLORICH database (Hartmann et al., 2019) indicates that our model can
600 basically capture the TOC and DOC concentrations in European rivers (Figs 4, 5, S7 and S8).
601 The simulation results explain 34% and 32% of the inter-site variation of the observed TOC and
602 DOC concentrations, respectively (Fig. 4). For major European rivers, such as the Rhine, Elbe,
603 Danube, Spree and Weser, the simulated long-term average TOC and DOC concentrations are
604 overall close to the observations (Fig. 5, S7 and S8). But for the Rhone river in southern France,
605 the DOC concentrations have been systematically overestimated by more than 50% (Fig. 5 and
606 S8m). In addition, both simulated and observed TOC and DOC concentrations show drastic
607 temporal (both seasonal and interannual) variations (Figs 4, S7 and S8). Our model seems to
608 have overestimated the temporal variation of TOC and especially DOC concentrations (Figs S7
609 and S8).

https://doi.org/10.5194/esd-2022-4
Preprint. Discussion started: 1 February 2022

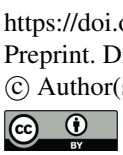

Earth System Dynamics
Discussions
Open Access
EGU

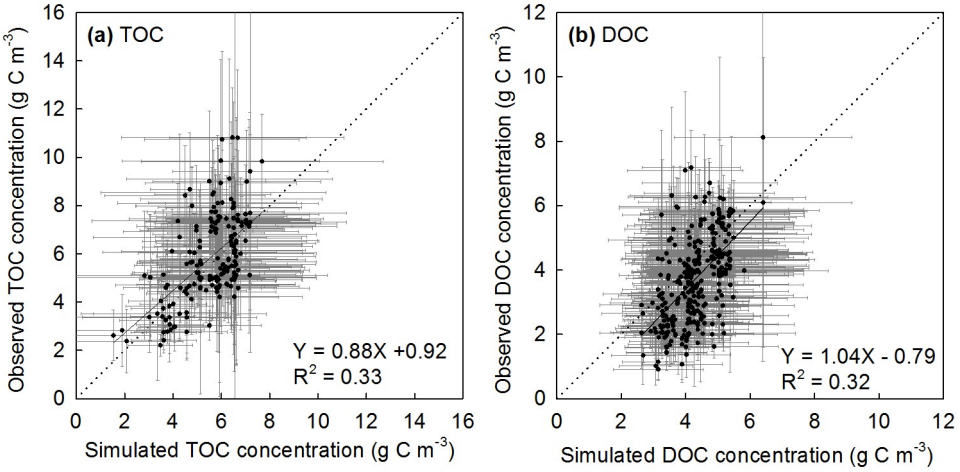

610

611 **Figure 4** Comparison between the observed and simulated riverine TOC (a, POC+DOC) and
612 DOC (b) concentrations. The dot and error bar denote the mean and standard deviation at each
613 gauging site, respectively. Not that the mean and standard deviation of the simulated
614 concentrations at each site are calculated based on the monthly average value, but the mean and
615 standard deviation of the observed concentrations are based on instantaneous observation.

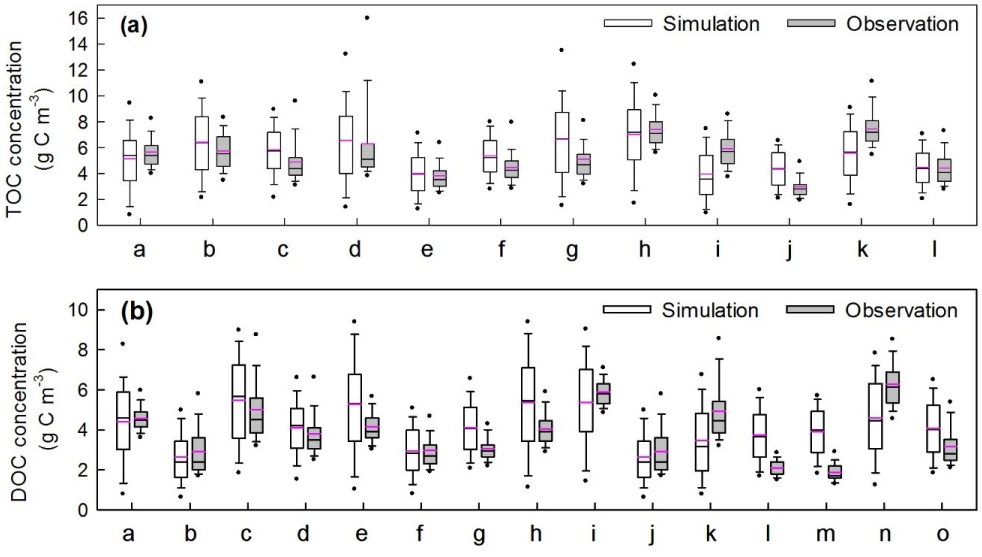

616

617 **Figure 5** Comparison between the observed and simulated concentrations of total organic carbon
618 (TOC, a) and dissolved organic carbon (DOC, b) in river flows. The black and pink lines in each
619 box denote the median and mean value, respectively. Box boundaries show the 25th and 75th

https://doi.org/10.5194/esd-2022-4
Preprint. Discussion started: 1 February 2022


Earth System Dynamics Discussions

620 percentiles, whiskers denote the 10th and 90th percentiles, the dots below and above each box
621 denote the 5th and 95th percentiles, respectively. The specific gauging station represented by a-o
622 in figure (a) and (b) can be found in the corresponding sub-plot in Figure S7 and S8,
623 respectively.

624

625 In Europe, the GLORICH database only provides POC concentrations measured at three gauging
626 stations in northwestern Germany (Figs. 6, S2d). The simulated POC concentrations in the Ems
627 river at Rheine are overall comparable to the observation (Fig. 6e, f). However, at the two
628 gauging sites at the river Rhine, the POC concentrations have been significantly underestimated
629 (Figs. 6a-d). We noticed that the stream routing scheme of Rhine catchment at 0.5° obtained
630 from the forcing data STN-30p (Vörösmarty et al., 2000) differs significantly from the stream
631 routing scheme extracted based on high resolution (3″) DEM. Thus, besides the errors in
632 simulated SOC stocks, soil erosion rate, stream discharge rate, and sediment transport and
633 deposition rate, the inaccurate stream routing scheme used in this study might also be an
634 important reason for the underestimation of POC concentration in Rhine river.

https://doi.org/10.5194/esd-2022-4
Preprint. Discussion started: 1 February 2022

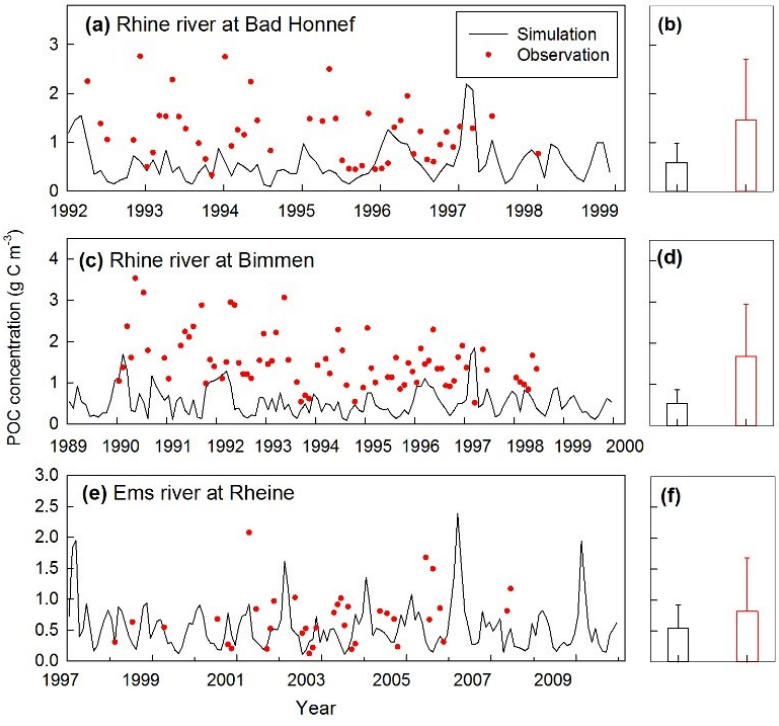

635

636 **Figure 6** Comparison between the observed (instantaneous measurement) and simulated
637 (monthly average value) riverine POC concentrations at three gauging sites. In figure (b), (d) and
638 (f), the histogram and error bar denote the mean and standard deviation of POC concentrations,
639 respectively.

640

641 **3.2 Lateral carbon transfers in Europe**

642 Based on our simulation results, the average annual sediment delivery from upland to the river
643 network caused by water erosion in Europe (-30W– 70E, 34N-75N) during 1901-2014 is 2.8±0.4
644 Pg yr^{-1} (Fig. 7a). From Northern to Southern Europe, the sediment delivery rate from upland to
645 river increase from less than 1.0 g m^{-2} yr^{-1} in the Scandinavia Peninsula, which is covered by
646 mature boreal forests (Fig. S9a), and in the Northern European Plain to more than 600 g m^{-2} yr^{-1}
647 in the mountainous regions of the Apennine Peninsula, Balkan Peninsula and the Middle East
648 (Figs. 8a, S10a). The Caucasus is mainly covered by ice and bare rock (Fig. S9), thus the
649 sediment delivery rate in this region is also very low. In total across Europe, 55.2% (1.8±0.2 Pg

https://doi.org/10.5194/esd-2022-4
Preprint. Discussion started: 1 February 2022

Earth System Dynamics
Discussions
Open Access
EGU

650 yr^{-1}) of the sediment delivered into river network is deposited in river channels and floodplains,
651 and the remaining 36.8% (1.0±0.1 Pg yr^{-1}) is exported to the sea (Fig. 7a). Generally, large
652 rivers, like Danube, Volga, and Ob rivers, carry more sediment to the sea than small rivers (Figs.
653 8b, c). But several relatively small rivers in the Middle East and the Po river in northern Italy
654 also carry similarly large amount of sediment to the sea, as the upland soil erosion rates are very
655 high (> 200 g m^{-2} yr^{-1}) in these catchments (Figs. 8a, c). Spatial distribution of the sediment
656 deposition is controlled by the stream routing scheme and the spatial distribution of floodplains
657 (Fig. 9b). In Northern and Central Europe, the area-averaged sediment deposition rates (i.e.
658 amount of annual sediment deposition /area of 0.5°×0.5° grid cell) in river channels and
659 floodplains are mostly less than 100.0 g m^{-2} yr^{-1} (Fig. 8d). In the downstream part of the Danube,
660 Po and several rivers in the Middle East, the sediment deposition rate can exceed 800.0 g m^{-2} yr^{-1}. From 1901 to 1960s, the annual total sediment delivery from uplands to the whole river
662 network of Europe declined from about 3.0 Pg yr^{-1} to about 2.3 Pg yr^{-1} (Fig. S11a). From 1960 to
663 2014, the annual sediment delivery rate did not show a significant trend, but revealed large
664 interannual variations.

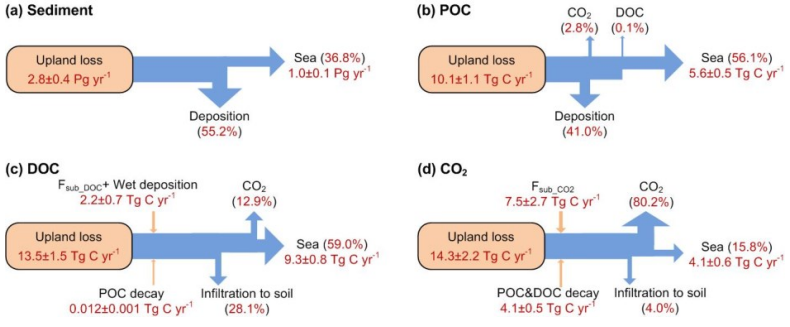

665

666 **Figure 7** Averaged annual lateral redistribution rate of sediment (a), POC (b), DOC (c) and CO_2
667 (d) in Europe for the period 1901-2014. F_{sub_DOC} and F_{sub_CO2} are the DOC and CO_2 inputs from
668 floodplain soil (originated from the decomposition of submerged litter and soil carbon) to the
669 overlying flooding water, respectively.

https://doi.org/10.5194/esd-2022-4
Preprint. Discussion started: 1 February 2022

Earth System Dynamics
Discussions
Open Access
EGU

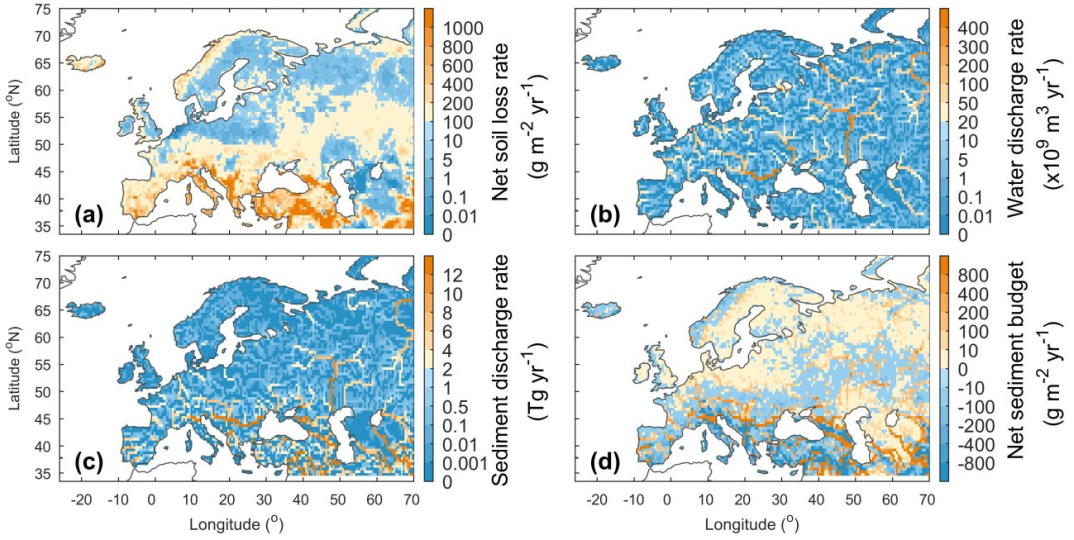

Figure 8 Averaged annual lateral redistribution rate of water and sediment in Europe during 1901-2014. (a) Annual sediment delivery rate from upland to river network; (b) annual water discharge rate; (c) annual sediment discharge rate and (d) annual net sediment budget in each 0.5°×0.5° grid cell. In figure d, the positive and negative values denote net gain and net loss of sediment, respectively.

Along with soil erosion and sediment transport, the average annual POC delivery from upland to river network in the whole Europe during 1901-2014 is 10.1±1.1 Tg C yr^{-1} (Fig. 7b). 41.0% of the POC delivered into the river network is deposited in river channels and floodplains, 2.9% is decomposed during transport, and the remaining 56.1% is exported to the sea. Spatial patterns of the area-averaged SOC delivery rate and POC discharge rate basically follow that of sediment (Fig. 9a, c). But although the sediment discharge rates in some small rivers in the Middle East can be as high as that in the Danube or Volga river (Fig. 8c), the POC delivery rates in these small rivers is much smaller than in the larger ones (Fig. 9c). This is mainly due to the lower SOC stocks in the Middle East compared to those found in the Danube and Volga catchments (Fig. S6). We also note that different from the sediment delivery, the annual total POC delivery from upland to river network in Europe did not show a significant declining trend from 1901 to 1960s (Fig. S11b). The increase in SOC stock (Fig. S11c) may have partially offset the decline in sediment delivery rate.

https://doi.org/10.5194/esd-2022-4
Preprint. Discussion started: 1 February 2022

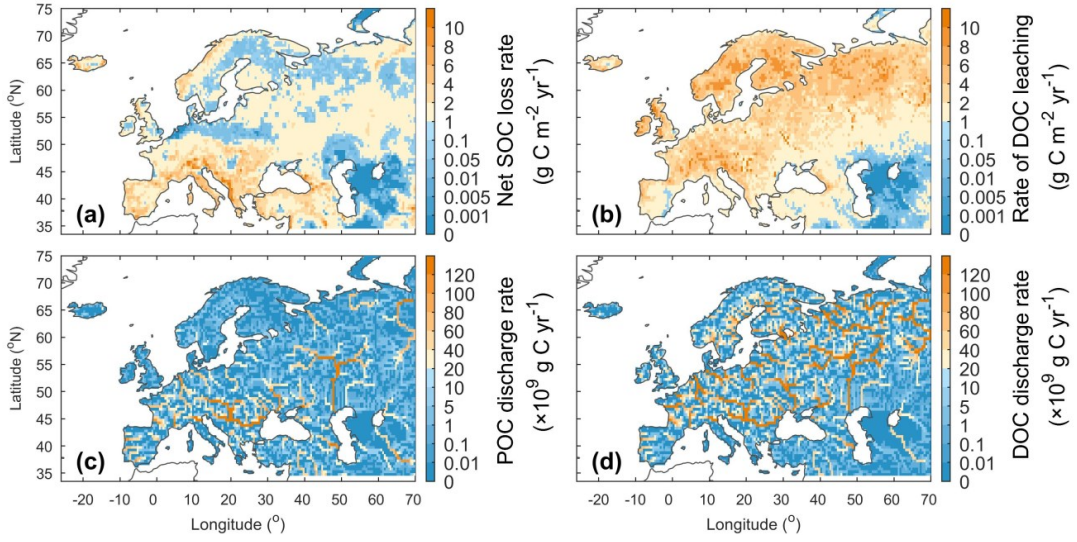

690

691 **Figure 9** Averaged annual lateral redistribution rate of organic carbon in Europe during 1901-
692 2014. (a) Annual SOC delivery rate from upland to river network; (b) annual DOC leaching rate;
693 (c) annual POC discharge rate and (d) annual DOC discharge rate.

694

695 Leaching results in an average annual DOC input of 13.5±1.5 Tg C yr^{-1} from soil to the river
696 network in Europe, and the *in-situ* DOC production caused by wet deposition and the
697 decomposition of riverine POC and submerged litter and soil organic carbon under flooding
698 waters amounts to 2.2±0.7 Tg C yr^{-1} (Fig. 7c). 28.1% of the total riverine DOC is then infiltrating
699 into the floodplain soils, 12.9% is decomposed during riverine transport, and the remaining
700 59.0% is exported to the sea. The spatial distribution of the DOC leaching rate is very different
701 from that of POC (Fig. 9b). From North-western Europe to Southeast Europe and the Middle
702 East, the DOC leaching rates decrease from over 6 g C m^{-2} yr^{-1} to less than 1.0 g C m^{-2} yr^{-1}. DOC
703 discharge rates in major European rivers, such as Rhine, Danube, Volga, Elbe and Ob, are mostly
704 higher than 100 Tg C yr^{-1} (Fig. 9d). Comparatively, the DOC discharge rates in Southern Europe
705 and the Middle East are significantly lower (<60 Tg C yr^{-1}).

706 The average annual leaching rate of CO_2 sourced from the decomposition of upland litter and
707 soil organic carbon (incl. DOC) in the whole Europe is 14.3±2.2 Tg C yr^{-1} (Fig. 7a).
708 Decomposition of the submerged litter and organic carbon in floodplains and the decomposition

https://doi.org/10.5194/esd-2022-4
Preprint. Discussion started: 1 February 2022

Earth System Dynamics Discussions

of riverine POC and DOC add an an *in-situ* CO_2 production amounting to 7.5±2.7 Tg C yr^{-1} and 4.1±0.5 Tg C yr^{-1}, respectively. Most of this CO_2 (80.2%) feeding stream waters is then released back to the atmosphere quickly, in such a way that only 15.8% of the CO_2 is exported to the sea, and 4.0% is infiltrated into the floodplain soils.

3.3 Implications for the terrestrial C budget of Europe

Representing the lateral carbon transport in LSM is helpful to estimate the terrestrial carbon cycle more accurately. From the year 1901 to 2014, soil erosion and leaching combined resulted in a 5.4 Pg loss of terrestrial carbon to the European river network, this amount corresponding to about 5% of the total SOC stock (106 Pg C, Fig. S6a) in the 0-30 cm soil layer. The average annual total delivery of organic carbon (POC+DOC) during the same period is 47.3±6.6 Tg C yr^{-1} (Fig. 7), which is about 4.7% of the net ecosystem exchange (NEE (993±255 Tg C yr^{-1}), defined as the difference between the vegetation primary production (NPP) and the soil heterotrophic respiration (Rh) due to the decomposition of litter and soil organic matter (i.e. NEE=NPP–Rh)), and 19.2% of the net biome production (NBP (243±189 Tg C yr^{-1}), defined as the difference between NEP and the land carbon loss (Rd) due to the additional disturbances (e.g. harvest, land cover change, and soil erosion and leaching, i.e. NBP=NEP–Rd–DOC and POC to river) (Fig. 10b). The annual total export of carbon to the sea surrounding Europe is 19.0±1.4 Tg C yr^{-1}, which amounts to 1.9% and 8.7% of the NEE and NBP, respectively.

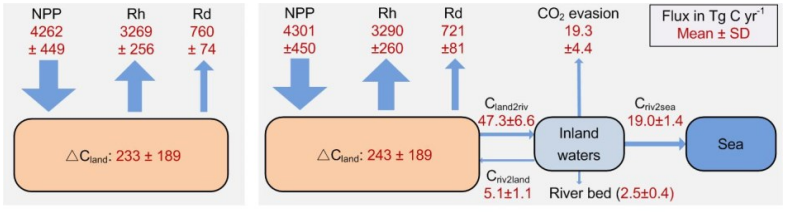

Figure 10 The simulated average annual carbon budget of the terrestrial ecosystem in Europe during the 1901-2014 when the lateral carbon transport is ignored (a) and considered (b). All fluxes are presented as mean ± standard deviation. NPP is the net primary production. Rh and Rd are the heterotrophic respiration and the respiration due to disturbances like harvest and land cover change, respectively. ΔC_{land} is the average annual changes of the total land carbon stock. Percentage following each of these changes in blue is the average annual relative changes of the

https://doi.org/10.5194/esd-2022-4
Preprint. Discussion started: 1 February 2022


Earth System Dynamics Discussions

734 corresponding carbon pool. $C_{land2riv}$, $C_{riv2land}$ and $C_{riv2sea}$ are the average annual carbon fluxes
735 from land to inland waters, from inland waters to river and from inland waters to the sea,
736 respectively. SD is the standard deviation.

737

738 Besides direct transfers of organic carbon from soil to aquatic systems, the lateral transport of
739 water, sediment and carbon can also affect the land carbon budget through several indirect ways.
740 First, the lateral redistribution of surface runoff can affect the land carbon budget by altering soil
741 wetness. Our simulation results reveal that the lateral redistribution of runoff can significantly
742 change local soil wetness, especially in floodplains (Fig. S10b), where the increase in soil
743 wetness can be larger than 10% (Fig. S13b). Soil wetness is a key controlling factor of plant
744 photosynthesis (Knapp et al., 2001; Stocker et al., 2019; Xu et al., 2013). Benefiting from the
745 increase in soil wetness, the NPP in many grid cells with a large area of floodplain has increased
746 by more than 5% (Fig. 10b), although the NPP over the whole Europe only increased by 1%
747 (Fig. 10). Changes in soil wetness can further alter soil temperature (Fig. S13a). As soil wetness
748 and temperature are the two most important controlling factors of organic matter decomposition,
749 the lateral redistribution of runoff can affect local land carbon budget by changing the Rh.
750 Moreover, in ORCHIDEE-$C_{lateral}$, the turnover times of litter and SOC under flooding waters are
751 set to be three times of the litter and SOC turnover times in upland soil (Reddy & Patrick Jr,
752 1975; Neckles & Neill, 1994; Lauerwald et al., 2017). Accounting for flooding thus decreases
753 the decomposition rate of litter and SOC stored in floodplain soils.

754 Second, soil erosion and sediment deposition can affect land carbon budget by altering the
755 vertical distribution of litter and soil organic carbon. At the net erosion sites of the uplands, the
756 loss of surface soil results in a part of the belowground litter and SOC that were originally stored
757 in deeper soil layers emerging to the surface soil layers, and also results in a fraction of the
758 belowground litter becoming the aboveground litter. In the floodplains, the newly deposited
759 sediment becomes the new surface soil layer, and the belowground litter and SOC in the original
760 surface soil layer is transferred down to the deeper soil layers. As the temperatures and fresh
761 organic matter inputs (sourced from the aboveground litterfall and dead roots), which can impact
762 SOC decomposition rates through the priming effect (Guenet et al., 2016; Guenet et al., 2010), in
763 different soil layers are different, changes in the vertical distribution of belowground litter and

https://doi.org/10.5194/esd-2022-4
Preprint. Discussion started: 1 February 2022

764 SOC can therefore lead to changes in the overall decomposition rate of the organic matter in the
765 whole soil column.

766 Third, soil aggregates mostly break down during soil erosion and sediment transport, the riverine
767 POC thus loses part of its physically protection from decomposition (Hu and Kuhn, 2016; Lal,
768 2003). Some modelling studies have assumed that at least 20% of the eroded SOC would be
769 decomposed during the soil erosion and transport processes (Lal, 2003, 2004; Zhang et al.,
770 2014). However, the estimation by Smith et al. (2001) using a conceptual mass balance model
771 suggest that only a tiny fraction of the eroded POC is decomposed and released as CO_2 to the
772 atmosphere. Using laboratory rainfall-simulation experiments, van Hemelryck et al. (2010)
773 estimated a 2%-12% mineralization of the eroded SOC from a loess soil, and Wang et al. (2014)
774 estimated a mineralization of only 1.5%. In ORCHIDEE-$C_{lateral}$, the passive SOC pool is
775 regarded as the SOC associated to soil minerals and protected by soil aggregates. The turnover
776 time of the passive POC in river stream and flooding waters is assumed to be same to that of the
777 active POC (0.3 year). Our simulation results suggest that the fraction of total riverine POC that
778 is decomposed during the lateral transport from uplands to the sea is 2.9% in Europe (Fig. 7b),
779 and the acceleration of POC decomposition rate due to the breakdown of soil aggregates can thus
780 slightly affect the estimate of the regional land-atmosphere carbon flux. Moreover, the riverine
781 POC and DOC can be transported over a long distance and finally settle or infiltrate in
782 floodplains or river channels (especially the Estuarine deltas) where the local environmental
783 conditions might be quite different from those encountered in the uplands from where these C
784 pools originate. These changes in environmental conditions can affect the decomposition rate of
785 the laterally redistributed organic carbon (Abril et al., 2002).

786 Comparison between the simulation results from ORCHIDEE-$C_{lateral}$ with activated and
787 deactivated erosion and river routing modules indicate that the ignoring of lateral carbon
788 transport processes in LSM may lead to significant biases in the simulated land carbon budget
789 (Figs. 10 and S11). Although the omission of lateral carbon transport in ORCHIDEE-$C_{lateral}$ only
790 resulted in a 1% decrease in simulated average annual total NPP in Europe during 1901-2014
791 and a 1% increase of annual total Rh, the annual total NBP (=NPP–Rh–Rd–DOC and POC to
792 river) is underestimated by 4.5%. Over the same period, the lateral carbon transport only induced
793 a 0.09% increase in the total SOC and DOC stock in Europe (Fig. S12c), but their spatial

https://doi.org/10.5194/esd-2022-4
Preprint. Discussion started: 1 February 2022

Earth System Dynamics Discussions
Open Access
EGU

794 distribution was significantly altered (Figs. 11e,f). For instance, in some mountainous regions,
795 the soil erosion induced a reduction of the SOC stock by more than 8%. On the contrary, the
796 sediment and POC deposition in some floodplains led to an increase in SOC stock by more than
797 8% (Fig. 11f).

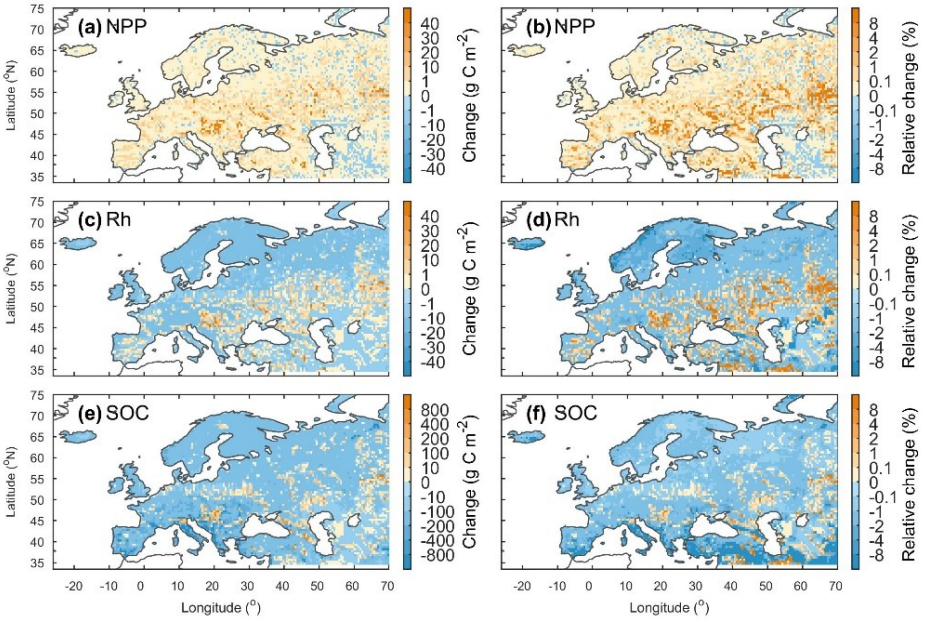

798

799 **Figure 11** Changes (first column) and relative changes (second column) of the net primary
800 production (NPP), heterotrophic respiration (Rh) and total soil organic carbon (SOC, 0-2 m) in
801 Europe due to the lateral carbon transport during 1901-2014. For each variable, the change is
802 calculated as C_{lat} - C_{nolat}, where C_{lat} and C_{nolat} are the carbon fluxes or stocks when lateral carbon
803 transport is considered and ignored, respectively. The relative changes is calculated as (C_{lat} -
804 C_{nolat}) / C_{nolat} × 100%.

805

806 **3.4 Persisting short comings and future work**

807 Although most processes related to lateral carbon transport have been represented in
808 ORCHIDEE-$C_{lateral}$, there are still omitted processes and large uncertainties in our model. For
809 example, many studies suggest that a substantial portion of the eroded sediment and carbon is
810 deposited downhill at adjacent lowlands as colluviums, rather than exported to the river (Berhe et

https://doi.org/10.5194/esd-2022-4
Preprint. Discussion started: 1 February 2022

al., 2007; Smith et al., 2001; Stallard, 1998; Wang et al., 2010). As the deposition of sediment and carbon within headwater basins can also significantly alter the vertical SOC profile and soil micro-environments (e.g. soil moisture, aeration and density) (Doetterl et al., 2016; Gregorich et al., 1998; Wang et al., 2015; Zhang et al., 2016), omission of this process may result in uncertainties in the simulated vegetation production and SOC decomposition. In addition, the impact of artificial dams and reservoirs on riverine sediment and carbon fluxes is also not represented in our model. Construction of dams generally leads to increased water residence time, nutrient retention, and sediment and carbon trapping in the impounded reservoir (Maavara et al., 2017), and can also affect the downstream flooding regime and frequency (Mei et al., 2016; Timpe and Kaplan, 2017). Estimation from Maavara et al. (2017) suggests that the organic carbon trapped or mineralized in global artificial reservoirs is about 13% of the total organic carbon carried by global rivers to the oceans. To more accurately simulate the lateral carbon transport, we plan to include the soil and carbon redistribution within headwater basins and the effects of dams and reservoirs on riverine sediment and carbon fluxes into our model in the near future.

The effects of lateral redistribution of water and sediment on vegetation productivity has not been fully represented in our model. As shown above, our model is able to represent the impacts of lateral water redistribution on vegetation productivity though modifying local soil wetness (Figs. 11 and S13). However, in addition to modifying soil wetness, many studies have indicated that the soil erosion and sediment deposition can affect vegetation productivity by modifying soil nutrient (e.g. e.g. nitrogen (N) and phosphorus (P)) availability (Bakker et al., 2004; Borrelli et al., 2018; Quine, 2002; Quinton et al., 2010). Recently, terrestrial N and P cycles have already been incorporated into another branch of ORCHIDEE (i.e. the ORCHIDEE-CNP developed by Goll et al., 2017). By coupling our new branch and ORCHIDEE-CNP, it will be possible to develop a more comprehensive LSM that can also simulate the effects of lateral N and P redistribution on vegetation productivity.

Although soils are the major source of riverine organic carbon, domestic, agricultural and industrial wastes, as well as the river-borne phytoplankton can also make significant contributions (Abril et al., 2002; Meybeck, 1993). Moreover, previous studies have shown that sewage generally contains highly labile POC and most of the aquatic production can be

https://doi.org/10.5194/esd-2022-4
Preprint. Discussion started: 1 February 2022

841 mineralized within a short time (Abril et al., 2002; Caffrey et al., 1998). Omission of organic
842 carbon inputs from manure, sewage and river-borne phytoplankton may be one of the main
843 reasons for the underestimation of CO_2 evasion in the European river network, compared to the
844 estimates using statistical models based on observed riverine DOC concentrations (Lauerwald et
845 al., 2015; Raymond et al., 2013). Inclusion of these additional carbon sources should thus help
846 reconcile simulated and observed riverine carbon concentrations and aquatic CO_2 evasion.

847 Uncertainties in our simulation results also stem from the forcing data (Table 1) applied in our
848 model. The routing scheme of water, sediment and carbon is driven by a map of stream flow
849 direction at 0.5° spatial resolution (Guimberteau et al., 2012). Comparison between this flow
850 direction map and the flow direction map derived based on high resolution (3″) DEM show
851 discrepancies between the two river flow networks (Fig. S5). As the flow direction directly
852 determines the area of each catchment and the route of river flows, errors in forcing data of flow
853 direction may thus induce uncertainties in the simulated riverine water, sediment and carbon
854 discharges. Land-cover maps are another source of uncertainty. For instance, croplands generally
855 experience significantly larger soil erosion rates than grasslands and forests (Borrelli et al., 2017;
856 Nunes et al., 2011; Zhang et al., 2020). However, croplands in ORCHIDEE are only represented
857 in a simplified way by segmenting them into C3 and C4 crops based on their photosynthesis
858 characteristics. Therefore, our simulations based on land cover data with only two broad groups
859 of crop might not be able to fully capture the seasonal dynamics of planting, canopy growth rate
860 and harvesting for all crop types. Furthermore, the effects of soil conservation practices, which
861 would decrease erosion rates, are ignored in our model. Panagos et al. (2015) have shown that
862 contour farming, stone wall and grass margin techniques have been applied in Europe reduce the
863 risk of soil erosion. However, these soil conservation practices only reduce the average erosion
864 rate in European Union by 3%. Excluding soil conservation practices thus should have limited
865 impact in our simulation results.

866 Further model calibration and evaluation, especially using observation data from regions outside
867 of Europe, is necessary. In ORCHIDEE-$C_{lateral}$, an empirical equation (Eq. 8) adapted from the
868 WBMsed model, which was originally proposed to simulate the total suspended sediment
869 discharge in global rivers (Cohen et al., 2014), is used to estimate the transport capacities of clay,
870 silt and sand sediment. By calibrating the parameters controlling sediment transport capacity and

https://doi.org/10.5194/esd-2022-4
Preprint. Discussion started: 1 February 2022

the deposition rate of excess suspended sediment (Table A1) against observed sediment discharge rate in major European rivers (e.g. Rhine and Danube river), our model can overall capture the sediment discharge rate in many European rivers (Fig. 3). Even so, there are still large uncertainties in the simulated sediment discharge rate (Fig. 3), and it is unknown whether our model would perform satisfactorily in regions with very different climates than Europe (such as in the tropical regions). Thus, in the future, the aim is to extend the model applications to contrasted regions or even the globe to refine the calibration of model parameters and evaluate its ability to on predict the lateral sediment and carbon transport across a wide range of climate regimes and terrestrial biomes. Moreover, the GLORICH database (Hartmann et al., 2019) only provides instantaneous observations of riverine organic carbon concentrations and it is therefore difficult to evaluate the model performance at annual or decadal scales. Therefore, future modelling efforts should be combined with a data mining effort targeting the collection of more continuous (e.g. daily) and long-term observational data of organic carbon content and fluxes in streams and rivers.

Conclusions

By merging ORCHILEAK (Lauerwald et al., 2017) and an upgraded version of ORCHIDEE-MUSLE (Zhang et al., 2020) for the simulation of DOC and POC from land to sea, respectively, we developed ORCHIDEE-$C_{lateral}$, a new branch of the ORCHIDEE LSM. ORCHIDEE-$C_{lateral}$ simulates the large-scale lateral transport of water, sediment, POC, DOC and CO_2 from uplands to the sea through river networks, the deposition of sediment and POC in river channels and floodplains, the decomposition POC and DOC during fluvial transport and the CO_2 evasion to the atmosphere, as well as the changes in soil wetness and vertical SOC profiles due to the lateral redistribution of water, sediment and carbon.

Evaluation using observation data from European rivers indicate that ORCHIDEE-$C_{lateral}$ can satisfactorily reproduce the observed riverine discharges of water and sediment, bankfull flows and organic carbon concentrations in river flows. Application of ORCHIDEE-$C_{lateral}$ to the entire European river network from 1901 to 2014 reveals that the average annual total carbon delivery to streams and rivers amounts to 47.3±6.6 Tg C yr^{-1}, which corresponds to about 4.7% of total NEP and 19.2% of the total NBP of terrestrial ecosystems in Europe. The lateral transfer of

https://doi.org/10.5194/esd-2022-4
Preprint. Discussion started: 1 February 2022


Earth System Dynamics Discussions Open Access EGU

water, sediment and carbon can affect the land carbon dynamics through several different mechanisms. Besides directly inducing a spatial redistribution of organic carbon, it can also affect the regional land carbon budget by altering vertical SOC profiles, as well as the soil wetness and soil temperature, which in turn impact vegetation production and the decomposition of soil organic carbon. Overall, omission of lateral carbon transport in ORCHIDEE potentially results in an underestimation of the annual mean NBP in Europe of 4.5%. In regions experiencing high soil erosion or high sediment deposition rate, the lateral carbon transport also changes total SOC stock significantly, by more than 8%.

We recognize that ORCHIDEE-$C_{lateral}$ is still entailed with several limitations and significant uncertainties. To address those, we plan to enhance our model with additional processes, such as sediment deposition at downhills or the regulation of lateral transport by dams and reservoirs. We also plan to calibrate and evaluate further our model by extending the observational dataset to regions outside Europe.

https://doi.org/10.5194/esd-2022-4
Preprint. Discussion started: 1 February 2022


Earth System Dynamics Discussions

Code and data availability

The source code of ORCHIDEE-Clateral model developed in this study is available online (https://doi.org/10.14768/f2f5df9f-26da-4618-b69c-911f17d7e2ed) from 22 July, 2019. All forcing and validation data used in this study are publicly available online. The specific sources for these data can be found in section Table 1.

Author contributions

HZ, RL and PR designed the study. HZ and RL conducted the model development and simulation experiments. PR, KV, PC, VN, BG and WY provided critical contribution to the model development and the design of simulation experiments. HZ conducted the model calibration, validation and the data analysis. RL, PR, PC, KV and BG provided support on collecting forcing and validation data. HZ, RL and PR wrote the manuscript. All authors contributed to interpretation and discussion of results and improved the manuscript.

Competing interests

The contact author has declared that neither they nor their co-authors have any competing interests.

Acknowledgements

HZ and PR acknowledges the ‘Lateral-CNP’ project (No. 34823748) supported by the Fonds de la Recherche Scientifique –FNRS and the VERIFY project that received funding from the European Union’s Horizon 2020 research and innovation program under grant agreement No. 776810. RL and PC acknowledge funding by the French state aid managed by the ANR under the "Investissements d'avenir" programme [ANR-16-CONV-0003_Cland]. P.R. received funding from the European Union’s Horizon 2020 research and innovation programme under Grant Agreement no. 101003536 (ESM2025 – Earth System Models for the Future).

https://doi.org/10.5194/esd-2022-4
Preprint. Discussion started: 1 February 2022

References:

Abotalib, A. Z., and Mohamed, R. S. A: Surface evidences supporting a probable new concept for the river systems evolution in Egypt: a remote sensing overview. Environ. Earth Sci., 69, 1621-1635, 2012.

Abrams, M., Crippen, R., and Fujisada, H.: ASTER Global Digital Elevation Model (GDEM) and ASTER Global Water Body Dataset (ASTWBD). Remote Sens., 12, 2020.

Abril, G., Nogueira, M., Etcheber, H., Cabecadas, G., Lemaire, E., and Brogueira, M. J.: Behaviour of organic carbon in nine contrasting European estuaries. Estuar., Coast. Shelf Sci., 54, 241-262, 2002.

Arnold, J. G., Williams, J. R., and Maidment, D. R.: Continuous-time water and sediment-routing model for large basins. J. Hydraul. Eng., 121, 171-179, 1995.

Bakker, M. M., Govers, G., and Rounsevell, M. D. A.: The crop productivity–erosion relationship: an analysis based on experimental work. Catena, 57, 55-76, 2004.

Battin, T. J., Luyssaert, S., Kaplan, L. A., Aufdenkampe, A. K., Richter, A., and Tranvik, L. J.: The boundless carbon cycle. Nat. Geosci.e, 2, 598-600, 2009.

Berhe, A. A., Harte, J., Harden, J. W., and Torn, M. S.: The Significance of the Erosion-induced Terrestrial Carbon Sink. BioScience, 57, 337-346, 2007.

Beusen, A. H. W., Dekkers, A. L. M., Bouwman, A. F., Ludwig, W., and Harrison, J.: Estimation of global river transport of sediments and associated particulate C, N, and P. Global Biogeochem. Cycles, 19, https://doi.org/10.1029/2005GB002453, 2005.

Borrelli, P., Robinson, D. A., Fleischer, L. R., Lugato, E., Ballabio, C., Alewell, C., Meusburger, K., Modugno, S., Schütt, B., Ferro, V., Bagarello, V., Oost, K. V., Montanarella, L., and Panagos, P.: An assessment of the global impact of 21st century land use change on soil erosion. Nat. Commun., 8, 2017.

Borrelli, P., Van Oost, K., Meusburger, K., Alewell, C., Lugato, E., and Panagos, P.: A step towards a holistic assessment of soil degradation in Europe: Coupling on-site erosion with sediment transfer and carbon fluxes. Environ. Res., 161, 291-298, 2018.

Caffrey, J. M., Coloern, J. E., and Grenz, C.: Changes in production and respiration during a spring phytoplankton bloom in San Francisco Bay, California, USA: implications for net ecosystem metabolism. Mar. Ecol. Prog. Ser., 172, 1-12, 1998.

Camino-Serrano, M., Guenet, B., Luyssaert, S., Ciais, P., Bastrikov, V., De Vos, B., Gielen, B., Gleixner, G., Jornet-Puig, A., Kaiser, K., Kothawala, D., Lauerwald, R., Peñuelas, J., Schrumpf, M., Vicca, S., Vuichard, N., Walmsley, D., and Janssens, I. A.: ORCHIDEE-SOM: modeling soil organic carbon (SOC) and dissolved organic carbon (DOC) dynamics along vertical soil profiles in Europe. Geosci. Model Dev., 11, 937-957, 2018.

Campoy, A., Ducharne, A., Cheruy, F., Hourdin, F., Polcher, J., and Dupont, J. C.: Response of land surface fluxes and precipitation to different soil bottom hydrological conditions in a general circulation model. J. Geophys. Res.: Atmos., 118, 10,725-710,739, 2013.

Castro, J. M., and Thorne, C. R.: The stream evolution triangle: Integrating geology, hydrology, and biology. River Res. Appl., 35, 315-326, 2019.

Chaplot, V. A. M., Rumpel, C., and Valentin, C.: Water erosion impact on soil and carbon redistributions within

https://doi.org/10.5194/esd-2022-4
Preprint. Discussion started: 1 February 2022


Earth System Dynamics Discussions

uplands of Mekong River. Global Biogeochem. Cycles, 19, GB4004, 2005.

Chappell, A., Baldock, J., and Sanderman, J.: The global significance of omitting soil erosion from soil organic carbon cycling schemes. Nat. Clim. Chang., 6, 187-191, 2016.

Chini, L. P., Hurtt, G. C., and Frolking, S.: Harmonized Global Land Use for Years 1500 – 2100, V1. Data set. Available on-line [http://daac.ornl.gov] from Oak Ridge National Laboratory Distributed Active Archive Center, Oak Ridge, Tennessee, USA, http://dx.doi.org/10.3334/ORNLDAAC/1248, 2014.

Ciais, P., Sabine, C., Bala, G., Bopp, L., Brovkin, V., Canadell, J., Chhabra, A., DeFries, R., Galloway, J., Heimann, M., Jones, C., Le Quéré, C., Myneni, R. B., Piao, S. L., and Thornton, P.: Carbon and Other Biogeochemical Cycles, in: Stocker, T. F., Qin, D., Plattner, G.-K., Tignor, M., Allen, S. K., Boschung, J., Nauels, A., Xia, Y., Bex, V., and Midgley, P. M. (Eds.), Climate Change 2013: The Physical Science Basis. Contribution of Working Group I to the Fifth Assessment Report of the Intergovernmental Panel on Climate Change Cambridge University Press, Cambridge, United Kingdom and New York, NY, USA, 2013.

Ciais, P., Yao, Y., Gasser, T., Baccini, A., Wang, Y., Lauerwald, R., Peng, S., Bastos, A., Li, W., Raymond, P. A., Canadell, J. G., Peters, G. P., Andres, R. J., Chang, J., Yue, C., Dolman, A. J., Haverd, V., Hartmann, J., Laruelle, G., Konings, A. G., King, A. W., Liu, Y., Luyssaert, S., Maignan, F., Patra, P. K., Peregon, A., Regnier, P., Pongratz, J., Poulter, B., Shvidenko, A., Valentini, R., Wang, R., Broquet, G., Yin, Y., Zscheischler, J., Guenet, B., Goll, D. S., Ballantyne, A. P., Yang, H., Qiu, C., and Zhu, D.: Empirical estimates of regional carbon budgets imply reduced global soil heterotrophic respiration. Natl. Sci. Rev., 8, https://doi.org/10.1093/nsr/nwaa145, 2021.

Cohen, S., Kettner, A. J., and Syvitski, J. P. M.: Global suspended sediment and water discharge dynamics between 1960 and 2010: Continental trends and intra-basin sensitivity. Glob. Planet. Change, 115, 44-58, 2014.

Cole, J. J., Prairie, Y. T., Caraco, N. F., McDowell, W. H., Tranvik, L. J., Striegl, R. G., Duarte, C. M., Kortelainen, P., Downing, J. A., Middelburg, J. J., and Melack, J.: Plumbing the Global Carbon Cycle: Integrating Inland Waters into the Terrestrial Carbon Budget. Ecosystems, 10, 172-185, 2007.

Coulthard, T. J., and Van de Wiel, M. J.: Modelling river history and evolution. Philosophical Transactions A Mathematical, Phys. Eng. Sci., 370, 2123-2142, 2012.

d'Orgeval, T., Polcher, J., and de Rosnay, P.: Sensitivity of the West African hydrological cycle in ORCHIDEE to infiltration processes, Hydrol. Earth Syst. Sci., 12, 1387–1401, https://doi.org/10.5194/hess-12-1387-2008, 2008.

Dirmeyerm, P. A., Gao, X., Zhao, M., Guo, Z., Oki, T., and Hanasaki, N.: GSWP-2: Multimodel Analysis and Implications for Our Perception of the Land Surface. Bull. Amer. Meteorol. Soc., 87, 1381-1398, 2006.

Doetterl, S., Berhe, A. A., Nadeu, E., Wang, Z., Sommer, M., and Fiener, P.: Erosion, deposition and soil carbon: A review of process-level controls, experimental tools and models to address C cycling in dynamic landscapes. Earth Sci. Rev., 154, 102-122, 2016.

Drake, T. W., Raymond, P. A., and Spencer, R. G. M.: Terrestrial carbon inputs to inland waters: A current synthesis of estimates and uncertainty. Limn.Oceanogr. Lett., 3, 132-142, 2018.

FAO/IIASA/ISRIC/ISSCAS/JRC: Harmonized World Soil Database (version 1.2), FAO, Rome, Italy and IIASA,

https://doi.org/10.5194/esd-2022-4
Preprint. Discussion started: 1 February 2022

1017 Laxenburg, Austria, 2012.
1018 Galy, V., France-Lanord, C., and Lartiges, B.: Loading and fate of particulate organic carbon from the Himalaya to
1019 the Ganga–Brahmaputra delta. Geochim. Cosmochim. Acta, 72, 1767-1787, 2008.
1020 Gassman, P. W., Sadeghi, A. M., and Srinivasan, R.: Applications of the SWAT Model Special Section: Overview
1021 and Insights. J. Environ. Qual., 43, 1-8, 2014.
1022 Gregorich, E. G., Greer, K. J., Anderson, D. W., and Liang, B. C.: Carbon distribution and losses: erosion and
1023 deposition effects. Soil Tillage Res., 47, 291-302, 1998.
1024 Guenet, B., Camino-Serrano, M., Ciais, P., Tifafi, M., Maignan, F., Soong, J. L., and Janssens, I. A.: Impact of
1025 priming on global soil carbon stocks. Glob. Change Biol., 24, 1873-1883, 2018.
1026 Guenet, B., Moyano, F. E., Peylin, P., Ciais, P., and Janssens, I. A.: (2016) Towards a representation of priming on
1027 soil carbon decomposition in the global land biosphere model ORCHIDEE (version 1.9.5.2). Geosci. Model
1028 Dev., 9, 841-855, 2016.
1029 Guenet, B., Neill, C., Bardoux, G., and Abbadie, L.: Is there a linear relationship between priming effect intensity
1030 and the amount of organic matter input? Appl. Soil Ecol., 46, 436-442, 2010.
1031 Guimberteau, M., Drapeau, G., Ronchail, J., Sultan, B., Polcher, J., Martinez, J. M., Prigent, C., Guyot, J. L.,
1032 Cochonneau, G., Espinoza, J. C., Filizola, N., Fraizy, P., Lavado, W., De Oliveira, E., Pombosa, R., Noriega,
1033 L., and Vauchel, P.: Discharge simulation in the sub-basins of the Amazon using ORCHIDEE forced by new
1034 datasets. Hydrol. Earth Syst. Sci., 16, 911-935, 2012.
1035 Guimberteau, M., Zhu, D., Maignan, F., Huang, Y., Yue, C., Dantec-Nédélec, S., Ottlé, C., Jornet-Puig, A., Bastos,
1036 A., Laurent, P., Goll, D., Bowring, S., Chang, J., Guenet, B., Tifafi, M., Peng, S., Krinner, G., Ducharne, A.,
1037 Wang, F., Wang, T., Wang, X., Wang, Y., Yin, Z., Lauerwald, R., Joetzjer, E., Qiu, C., Kim, H., and Ciais, P.:
1038 ORCHIDEE-MICT (revision 4126), a land surface model for the high-latitudes: model description and
1039 validation. Geosci. Model Dev., 11, 121-163, 2018.
1040 Hanson, P. C., Hamilton, D. P., Stanley, E. H., Preston, N., Langman, O. C., and Kara, E. L.: Fate of allochthonous
1041 dissolved organic carbon in lakes: a quantitative approach. PLoS One, 6, e21884, 2011.
1042 Haregeweyn, N., Poesen, J., Deckers, J., Nyssen, J., Haile, M., Govers, G., Verstraeten, G., and Moeyersons, J.:
1043 Sediment-bound nutrient export from micro-dam catchments in Northern Ethiopia. Land Degrad. Dev., 19,
1044 136-152, 2008.
1045 Hartmann, J., Lauerwald, R., and Moosdorf, N.: GLORICH - Global river chemistry database, in: PANGAEA (Ed.),
1046 2019.
1047 Hengl, T., de Jesus, J. M., MacMillan, R. A., Batjes, N. H., Heuvelink, G. B., Ribeiro, E., Samuel-Rosa, A.,
1048 Kempen, B., Leenaars, J. G., Walsh, M. G., and Gonzalez, M. R.: SoilGrids1km--global soil information based
1049 on automated mapping. PLoS One, 9, e105992, 2014.
1050 Hu, Y., Kuhn, N. J.: Erosion-induced exposure of SOC to mineralization in aggregated sediment. Catena, 137, 517-
1051 525, 2016.
1052 Janssens, I. A., Freibauer, A., Ciais, P., Smith, P., Nabuurs, G. J., Folberth, G., Schlamadinger, B., Hutjes, R. W.,
1053 Ceulemans, R., Schulze, E. D., Valentini, R., and Dolman, A. J.: Europe's terrestrial biosphere absorbs 7 to

https://doi.org/10.5194/esd-2022-4
Preprint. Discussion started: 1 February 2022


Earth System Dynamics Discussions

12% of European anthropogenic CO2 emissions. Science, 300, 1538-1542, 2003.

Jetten, V., Govers, G., Hessel, R.: Erosion models: quality of spatial predictions. Hydrol. Process., 17, 887-900, 2003.

Kalbitz, K., Schmerwitz, J., Schwesig, D., and Matzner, E.: Biodegradation of soil-derived dissolved organic matter as related to its properties. Geoderma, 113, 273-291, 2003.

Knapp, A. K., Briggs, J. M., and Koelliker, J. K.: Frequency and Extent of Water Limitation to Primary Production in a Mesic Temperate Grassland. Ecosystems, 4, 19-28, 2001.

Krinner, G., Viovy, N., de Noblet-Ducoudré, N., Ogée, J., Polcher, J., Friedlingstein, P., Ciais, P., Sitch, S., and Prentice, I. C.: A dynamic global vegetation model for studies of the coupled atmosphere-biosphere system. Global Biogeochem. Cycles, 19, 2005.

Lal, R.: Soil erosion and the global carbon budget. Environ. Int., 29, 437-450, 2003.

Lal, R.: Soil carbon sequestration impacts on global climate change and food security. Science, 304, 1623-1627, 2004.

Lauerwald, R., Laruelle, G., Hartmann, J., Ciais, P., and Regnier, P.: Spatial patterns in CO_2 evasion from the global river network: Spatial patter of riverine pCO2 and FCO2. Global Biogeochem. Cycles, 29, 2015.

Lauerwald, R., Regnier, P., Camino-Serrano, M., Guenet, B., Guimberteau, M., Ducharne, A., Polcher, J., and Ciais, P.: ORCHILEAK (revision 3875): a new model branch to simulate carbon transfers along the terrestrial–aquatic continuum of the Amazon basin. Geosci. Model Dev., 10, 3821-3859, 2017.

Lauerwald, R., Regnier, P., Guenet, B., Friedlingstein, P., and Ciais, P.: How Simulations of the Land Carbon Sink Are Biased by Ignoring Fluvial Carbon Transfers: A Case Study for the Amazon Basin. One Earth, 3, 226-236, 2020.

Lehner, B., Verdin, K., and Jarvis, A.: New global hydrography derived from spaceborne elevation data. Eos, Transactions, AGU, 89, 93-94, 2008.

Lugato, E., Paustian, K., Panagos, P., Jones, A., and Borrelli, P.: Quantifying the erosion effect on current carbon budget of European agricultural soils at high spatial resolution. Glob. Change Biol., 22, 1976-1984, 2016.

Luo, X., Li, H., Leung L.R., Tesfa, T. K., Getirana, A., Papa, F., and Hess L. L.: Modeling surface water dynamics in the Amazon Basin using MOSART-Inundation v1.0: impacts of geomorphological parameters and river flow representation. Geosci. Model Dev., 10, 1233-1259, 2017.

Maavara, T., Lauerwald, R., Regnier, P., and Van Cappellen, P.: Global perturbation of organic carbon cycling by river damming. Nat. Commun., 8, 15347, 2017.

Mei, X., Van Gelder, P., Dai, Z., and Tang, Z.: Impact of dams on flood occurrence of selected rivers in the United States. Front. Earth Sci., 11, 268-282, 2016.

Meybeck, M.: Riverine transport of atmospheric carbon: sources, global typology and budget. Water Air Soil Pollut., 70, 443-463, 1993.

Molinas, A., and Wu, B.: Transport of sediment in large sand-bed rivers. J. Hydraul. Res., 39, 135-146, 2001.

Moore, I. D., and Wilson, J. P.: Length-slope factors for the Revised Universal Soil Loss Equation: Simplified method of estimation. J. Soil Water Conserv., 47, 423-428, 1992.

https://doi.org/10.5194/esd-2022-4
Preprint. Discussion started: 1 February 2022


Earth System Dynamics Discussions

1091 Nadeu, E., de Vente, J., Martínez-Mena, M., and Boix-Fayos, C.: Exploring particle size distribution and organic
1092 carbon pools mobilized by different erosion processes at the catchment scale. J. Soils Sediments, 11, 667-678,
1093 2011.
1094 Naipal, V., Lauerwald, R., Ciais, P., Guenet, B., and Wang, Y.: CE-DYNAM (v1): a spatially explicit process-based
1095 carbon erosion scheme for use in Earth system models. Geosci. Model Dev., 13, 1201-1222, 2020.
1096 Nakhavali, M., Lauerwald, R., Regnier, P., Guenet, B., Chadburn, S., and Friedlingstein, P.: Leaching of dissolved
1097 organic carbon from mineral soils plays a significant role in the terrestrial carbon balance. Glob. Change Biol.,
1098 27, 1083-1096, 2021.
1099 Nardi, F., Annis, A., Di Baldassarre, G., Vivoni, E.R., and Grimaldi, S.: GFPLAIN250m, a global high-resolution
1100 dataset of Earth's floodplains. Sci. Data, 6, 180309, 2019.
1101 Nearing, M. A., Foster, G. R., Lane, L. J., and Finkner, S. C.: A Process-Based Soil Erosion Model for USDA-
1102 Water Erosion Prediction Project Technology. Transactions of the Asae, 32, 1587-1593, 1989.
1103 Neckles, H. A, and Neill, C.: Hydrologic control of litter decomposition in seasonally flooded prairie marshes.
1104 Hydrobiologia, 286, 155-165, 1994.
1105 Neitsch, S. L., Williams, J. R., Arnold, J. G., and Kiniry, J. R.: Soil and Water Assessment Tool Theoretical
1106 Documentation Version 2009. Texas Water Resources Institute, College Station, 2011.
1107 Nie, X., Li, Z., He, J., Huang, J., Zhang, Y., Huang, B., Ma, W., Lu, Y., and Zeng, G.: Enrichment of organic carbon
1108 in sediment under field simulated rainfall experiments. Environ. Earth Sci., 74, 5417-5425, 2015.
1109 Nodvin, S. C., Driscoll, C. T., and Likens, G. E.: Simple partitioning of anions and dissolved organic carbon in a
1110 forest soil. Soil Sci., 142, 27-35, 1986.
1111 Nunes, A. N., de Almeida, A. C., and Coelho, C. O. A.: (2011) Impacts of land use and cover type on runoff and soil
1112 erosion in a marginal area of Portugal. Appl. Geogr., 31, 687-699, 2011.
1113 Oeurng, C., Sauvage, S., and Sánchez-Pérez, J. M.: Assessment of hydrology, sediment and particulate organic
1114 carbon yield in a large agricultural catchment using the SWAT model. J. Hydrol., 401, 145-153, 2011.
1115 Parton, W. J., Schimel, D. S., Cole, C. V., and Ojima, D. S.: Analysis of Factors Controlling Soil Organic Matter
1116 Levels in Great Plains Grasslands1. Soil Sci. Soc. Am. J., 51, 1173-1179, 1987.
1117 Parton, W. J., Stewart, J. W. B., and Cole, C. V.: Dynamics of C, N, P and S in grassland soils: a model.
1118 Biogeochemistry, 5, 109-131, 1988.
1119 Polyakov, V. O., and Lal, R.: Soil organic matter and CO 2 emission as affected by water erosion on field runoff
1120 plots. Geoderma, 143, 216-222, 2008.
1121 Quine, T. A.: An investigation of spatial variation in soil erosion, soil properties and crop production with an
1122 agricultural field in Devon, UK. J. Soil Water Conserv., 57, 55-65, 2002.
1123 Quinton, J. N., Govers, G., Van Oost, K., and Bardgett, R. D.: The impact of agricultural soil erosion on
1124 biogeochemical cycling. Nat. Geosci., 3, 311-314, 2010.
1125 Raymond, P. A., Hartmann, J., Lauerwald, R., Sobek, S., McDonald, C., Hoover, M., Butman, D., Striegl, R.,
1126 Mayorga, E., Humborg, C., Kortelainen, P., Durr, H., Meybeck, M., Ciais, P., and Guth, P.: Global carbon
1127 dioxide emissions from inland waters. Nature, 503, 355-359, 2013.

https://doi.org/10.5194/esd-2022-4
Preprint. Discussion started: 1 February 2022

1128 Reddy, K. R., Patrick Jr, and W. H.: Effect of alternate aerobic and anaerobic conditions on redox potential, organic
1129 matter decomposition and nitrogen loss in a flooded soil. Soil Biol. Biochem., 7, 87-94, 1975.
1130 Regnier, P., Friedlingstein, P., Ciais, P., Mackenzie, F. T., Gruber, N., Janssens, I. A., Laruelle, G. G., Lauerwald,
1131 R., Luyssaert, S., Andersson, A. J., Arndt, S., Arnosti, C., Borges, A. V., Dale, A. W., Gallego-Sala, A.,
1132 Goddéris, Y., Goossens, N., Hartmann, J., Heinze, C., Ilyina, T., Joos, F., LaRowe, D. E., Leifeld, J., Meysman,
1133 F. J. R., Munhoven, G., Raymond, P. A., Spahni, R., Suntharalingam, P., and Thullner, M.: Anthropogenic
1134 perturbation of the carbon fluxes from land to ocean. Nat. Geosci., 6, 597-607, 2013.
1135 Sanderman, J., Hengl, T., and Fiske, G. J.: Soil carbon debt of 12,000 years of human land use. Proc. Natl. Acad.
1136 Sci., 114, 9575-9580, 2017.
1137 Schneider, C., Flörke, M., Eisner, E., and Voss, F.: Large scale modelling of bankfull flow: An example for Europe.
1138 J. Hydrol., 408, 235-245, 2011.
1139 Shangguan, W., Dai, Y., Duan, Q., Liu, B., and Yuan, H.: A global soil data set for earth system modeling. J. Adv.
1140 Model. Earth Syst., 6, 249-263, 2014.
1141 Sharpley, A. N., and Williams, J. R.: EPIC-erosion/productivity impact calculator: 2. User manual. Technical
1142 Bulletin - United States Department of Agriculture, 4, 206-207, 1990.
1143 Smith, S. V., Renwick, W. H., Buddemeier, R. W., and Crossland, C.J.: Budgets of soil erosion and deposition for
1144 sediments and sedimentary organic carbon across the conterminous United States. Global Biogeochem. Cycles,
1145 15, 697-707, 2001.
1146 Stallard, R. F.: Terrestrial sedimentation and the carbon cycle: Coupling weathering and erosion to carbon burial.
1147 Global Biogeochem. Cycles, 12, 231-257, 1998.
1148 Stocker, B. D., Zscheischler, J., Keenan, T. F., Prentice, I. C., Seneviratne, S. I., and Peñuelas, J.: Drought impacts
1149 on terrestrial primary production underestimated by satellite monitoring. Nat. Geosci., 12, 264-270, 2019.
1150 Telmer, K., and Veizer, J.: Carbon fluxes,pCO and substrate weathering in a large northern2river basin, Canada:
1151 carbon isotope perspectives. Chem. Geol., 159, 61-86, 1999.
1152 Tian, H., Yang, Q., Najjar, R. G., Ren, W., Friedrichs, M. A. M., Hopkinson, C. S., and Pan, S.: Anthropogenic and
1153 climatic influences on carbon fluxes from eastern North America to the Atlantic Ocean: A process-based
1154 modeling study. J. Geophys. Res.: Biogeosci., 120, 757-772, 2015.
1155 Timpe, K., and Kaplan, D.: The changing hydrology of a dammed Amazon. Sci. Adv., 3, 11, e1700611, 2017.
1156 Van Hemelryck, H., Govers, G., Van Oost, K., and Merckx, R.: Evaluating the impact of soil redistribution on the in
1157 situ mineralization of soil organic carbon. Earth Surf. Process. Landf., 36, 427-438, 2011.
1158 Van Oost, K., Quine, T. A., Govers, G., De Gryze, S., Six, J., Harden, J. W., Ritchie, J. C., McCarty, G. W.,
1159 Heckrath, G., Kosmas, C., Giraldez, J. V., da Silva, J. R., and Merckx, R.: The impact of agricultural soil
1160 erosion on the global carbon cycle. Science, 318, 626-629, 2007.
1161 Vigiak, O., Malago, A., Bouraoui, F., Vanmaercke, M., Obreja, F., Poesen, J., Habersack, H., Feher, J., and Groselj,
1162 S.: Modelling sediment fluxes in the Danube River Basin with SWAT. Sci. Total Environ., 599-600, 992-1012,
1163 2017.
1164 Vörösmarty, C. J., Fekete, B. M., Meybeck, M., and Lammers, R. B.: Geomorphometric attributesof the global

https://doi.org/10.5194/esd-2022-4
Preprint. Discussion started: 1 February 2022


Earth System Dynamics Discussions

1165 system of rivers at 30-minute spatial resolution. J. Hydrol., 237, 17-39, 2000.
1166 Wang, X., Cammeraat, E. L., Romeijn, P., and Kalbitz, K.: Soil organic carbon redistribution by water erosion--the
1167 role of CO2 emissions for the carbon budget. PLoS One, 9, e96299, 2014a.
1168 Wang, Z., Govers, G., Steegen, A., Clymans, W., Van den Putte, A., Langhans, C., Merckx, R., and Van Oost, K.:
1169 Catchment-scale carbon redistribution and delivery by water erosion in an intensively cultivated area.
1170 Geomorphology, 124, 65-74, 2010.
1171 Wang, Z., Hoffmann, T., Six, J., Kaplan, J. O., Govers, G., Doetterl, S., and Van Oost, K.: Human-induced erosion
1172 has offset one-third of carbon emissions from land cover change. Nat. Clim. Chang., 7, 345-349, 2017.
1173 Wang, Z., Van Oost, K., and Govers, G.: Predicting the long-term fate of buried organic carbon in colluvial soils.
1174 Global Biogeochem. Cycles, 29, 65-79, 2015.
1175 Wang, Z., Van Oost, K., Lang, A., Quine, T., Clymans, W., Merckx, R., Notebaert, B., and Govers, G.: The fate of
1176 buried organic carbon in colluvial soils: a long-term perspective. Biogeosciences, 11, 873-883, 2014b.
1177 Xu, X., Sherry, R. A., Niu, S., Li, D., and Luo, Y.: Net primary productivity and rain-use efficiency as affected by
1178 warming, altered precipitation, and clipping in a mixed-grass prairie. Glob. Change Biol., 19, 2753-2764, 2013.
1179 Yamazaki, D., Kanae, S., Kim, H., and Oki T.: A physically based description of floodplain inundation dynamics in
1180 a global river routing model. Water Resour. Res., 47, W04501, doi:10.1029/2010WR009726, 2011.
1181 Zhang, H., Lauerwald, R., Regnier, P., Ciais, P., Yuan, W., Naipal, V., Guenet, B., Van Oost, K., and Camino-
1182 Serrano, M.: Simulating Erosion-Induced Soil and Carbon Delivery From Uplands to Rivers in a Global Land
1183 Surface Model. J. Adv. Model. Earth Syst., 12, e2020MS002121, 2020.
1184 Zhang, H., Liu, S., Yuan, W., Dong, W., Xia, J., Cao, Y., and Jia, Y.: Loess Plateau check dams can potentially
1185 sequester eroded soil organic carbon. J. Geophys. Res. Biogeosci., 121, 2016.
1186 Zhang, H., Liu, S., Yuan, W., Dong, W., Ye, A., Xie, X., Chen, Y., Liu, D., Cai, W., and Mao, Y.: Inclusion of soil
1187 carbon lateral movement alters terrestrial carbon budget in China. Sci. Rep., 4, 7247, 2014.